LJMU Research Online

Azree Othuman Mydin, M, Hamah Sor, N, Bahrami, A, Dulaimi, A, Onuralp Özkılıç, Y, Althoey, F, Jagadesh, P, Isleem, HF and Tawfik, TA

 Residual durability, mechanical, and microstructural properties of foamed concrete subjected to various elevated temperatures

http://researchonline.ljmu.ac.uk/id/eprint/23917/

Article

http://researchonline.ljmu.ac.uk/

Residual durability, mechanical, and microstructural properties of foamed concrete subjected to various elevated temperatures

Md Azree Othuman Mydin [a,*], Nadhim Hamah Sor [b], Alireza Bahrami [c,*], Anmar Dulaimi [d,e], Yasin Onuralp Özkılıç [f,g], Fadi Althoey [h], P. Jagadesh [i], Haytham F. Isleem [j], Taher A. Tawfik [k,l]

[a] School of Housing, Building and Planning, Universiti Sains Malaysia, 11800 Penang, Malaysia
[b] Civil Engineering Department, University of Garmian, Kalar 46021, Kurdistan Region, Iraq
[c] Department of Building Engineering, Energy Systems and Sustainability Science, Faculty of Engineering and Sustainable Development, University of Gävle, 801 76 Gävle, Sweden
[d] Department of Civil Engineering, College of Engineering, University of Kerbala, Karbala 56001, Iraq
[e] Department of Civil Engineering, College of Engineering, University of Warith Al-Anbiyaa, Karbala 56001, Iraq
[f] Department of Civil Engineering, Faculty of Engineering, Necmettin Erbakan University, 42100 Konya, Turkey
[g] Department of Civil Engineering, Lebanese American University, Byblos, Lebanon
[h] Department of Civil Engineering, College of Engineering, Najran University, Najran, Saudia Arabia
[i] Department of Civil Engineering, Coimbatore Institute of Technology, Tamil Nadu 638 056, India
[j] Department of Construction Management, Qujing Normal University, Qujing 655011, Yunnan, China
[k] Department of Construction and Building Engineering, High Institute of Engineering, October 6 City, Egypt
[l] Institute of Construction and Architecture, Slovak Academy of Sciences, Dúbravská cesta 9, SK-845 03 Bratislava, Slovak Republic

ARTICLE INFO

ABSTRACT

Three different densities (500 kg/m^3, 1000 kg/m^3, and 1500 kg/m^3) of foamed concrete (FC) were tested alongside mortar with a density of 1980 kg/m^3 to investigate how high temperatures affect the qualities of FC. A flow table test was used to examine the fresh qualities of the mixtures. The modulus of elasticity, ultrasonic pulse velocity (UPV), bending strength, split tensile strength, compressive strength, thermal conductivity, porosity, and appearance and colour changes at ambient temperature and after exposure to various high temperatures (100 °C, 150 °C, 200 °C, 400 °C, 600 °C, and 800 °C) were evaluated. To study the effects of varying densities, microstructure analysis was performed utilizing scanning electron microscopy and mercury intrusion porosimetry. According to the findings, the four varied densities appeared dissimilar. FC with lower densities (500 kg/m^3 and 1000 kg/m^3) showed signs of cracking, while FC with a higher density (1500 kg/m^3) enabled for precise detection of the pore connectivity and surface spalling occurrences. High temperatures had less effect on the mortar than FC mixtures. As the temperature increased, the modulus of elasticity, split tensile strength, bending strength, compressive strength, thermal conductivity, and mass loss decreased for all the mortar and FC samples. The UPV values increased marginally up to 100 °C before decreasing. This investigation highlighted the need for additional research and code provisions that consider different innovative construction materials and FC constituent classes.

1. Introduction

Recently, the use of concrete in high-temperature applications has grown. High temperatures can severely damage concrete by causing physical and chemical alterations that substantially diminish its durability and mechanical characteristics [1]. Because of the chemical and physical changes caused by high temperatures, concrete deteriorates. Fire and high temperatures severely damage concrete, despite its greater heat resistance compared to other construction materials. When exposed to high temperatures, concrete undergoes many irreversible chemical and natural changes that can lead to the deterioration of the structural integrity of the concrete member, ultimately leading to the element's demise. The deterioration in physical form procedures accelerated by high temperatures has a major effect on the endurance of the concrete structure and can contribute to hazardous structural failures [2]. Elevated temperatures significantly influence the performance of

---

cement-based materials due to their constituent material characteristics. These characteristics include the void content and density of aggregates, as well as the thermal compatibility and adhesion of aggregate and cement paste [3–7].

Foamed concrete (FC) is classified as a type of lightweight concrete that is adaptable and innovative. It is a flexible building material because of its desirable properties, including low density, exceptional load-bearing capacity, minimal dimensional variation, and exceptional thermal insulation [8–11]. FC consists of at least 15% embedded foam within cement mortar, as well as pores of air enclosed within the matrix using a suitable surfactant [12]. The pores of air are created by mixing the air with a foaming agent that has been dissolved in water. The FC nature is obtained by gently combining the foam with the cement slurry [13]. Incorporating stable foam into the FC base mix yields a material with reduced self-weight. While stable foam improves insulating and workability characteristics compared to standard-strength concrete, it results in a reduction in the strength [14]. Therefore, FC can be produced in any region, despite its ultimate shape or dimension of the structure that includes it [15].

Compared to conventional concrete, FC production is both water- and energy-efficient [16,17]. By replacing part of concrete with bubbles of air [18,19], this creative method reduces the use of fine filler, cement, and water without causing damage to the environment. In recent years, there has been an increase in the use of FC as a semi-structural component in construction [20,21], taking advantage of its lightweight and efficient insulating properties. It is critical to note that many studies on FC have only examined its characteristics at ambient temperature. Most researchers believed that FC's mechanical properties have little effect on its thermal characteristics. There is an extreme lack of empirical evidence regarding the efficiency of fire barriers. However, these research projects provide a solid foundation for future studies on the mechanical properties of fire barriers at room temperature. Lin et al. [22] used stereomicroscopy and scanning electron microscopy (SEM) analysis to evaluate the microstructure of concrete that had undergone high temperatures. They found that moisture absorption from the surrounding environment can rehydrate dehydrated calcium oxide and ordinary Portland cement (OPC) grains, subsequently filling the voids. Schneider and Herbst [23] assessed non-evaporable water, C-H, CaCO$_3$, and C-S-H to investigate their behaviour and chemical reactions at various temperatures. They found that the considerable increase in the porosity, in addition to the permeability, observed within concrete at high temperatures [24], led to the opening of cracks, alterations in the material's internal structure, and microcracks owing to large gas levels. In addition to temperature, gas pressure, and moisture, the extent of concrete's cracking was also a factor in examining its permeability.

FC's degrading mechanisms are primarily responsible for the cementitious matrix's absence. Though deterioration of both chemical and mechanical properties results in a loss of mechanical properties, the temperatures at which these two processes function are quite distinct. The dehydration within cement paste gets substantial at temperatures above approximately 110 °C, thereby dramatically weakening the C-S-H bonds, which are characterised by the predominant formation within the cement paste's hydration [25]. Furthermore, the limited permeability of cement paste allows internal water pressure to accumulate during the C-S-H dehydration. At approximately 300 °C, this increases internal stresses and initiates microcracks, thereby reducing the stiffness and strength of the material. Above 450 °C, the calcium hydroxide dissociation leads FC to diminish [26]. Calcium oxide within FC transforms into calcium hydroxide while exposed to water at high temperatures, resulting in the chemical's destruction and cracking when employed in firefighting. Due to the challenge of accurately estimating these mechanisms, further research is necessary [27].

For a very long time, scientists have been interested in the FC's fire resistance. Kearsley and Mostert [28] investigated the way the type of cement influenced the high-temperature performance of FC. They discovered that FC produced with hydraulic cement containing calcium

oxide and aluminium oxide endured temperatures as high as 1,500 °C with no cracking. Othuman and Wang [29] suggested two methods for determining the FC's conductivity and thermal diffusivity at high temperatures. They also found that FC could serve as a substitute for gypsum in the construction of partition walls. High temperatures cause the internal pore structure of FC to deteriorate, leading to the degradation of durability properties. Therefore, it is crucial to study the changes in these characteristics to understand the buildings' response to fire [30]. Owing to the rise in the FC temperature, which ranges from 100 °C to 400 °C, the porosity and cracks in the micropore structure grow as a result of decarbonisation and water evaporation [31]. Beyond 400 °C, the decomposition and dehydration of hydration products are the primary causes of the resulting deterioration of the pore structure of concrete [32]. This leads to an increase in the void and a rise in the void diameter. Moreover, Tan et al. [33] evaluated residual characteristics of FC exposed to temperatures of 200 °C, 400 °C, and 600 °C with unit weights of 300 kg/m^3, 450 kg/m^3, 600 kg/m^3, and 800 kg/m^3. They noticed a downward trend in the mechanical and physical characteristics of FCs. However, the impact of temperatures up to 400 °C on FCs was not negligible. However, Bayraktar et al. [34] found that FC specimens with a 100 kg/m^3 foaming agent content outperformed specimens with a 50 kg/m^3 foaming agent content due to their higher void's ratio and solid content. Mydin and Wang [35] assessed the FC's physical characteristics subjected to temperatures as high as 600 °C. When exposed to temperatures as high as 600 °C, the FC maintained approximately 40% of its initial strength. The lightweight FC's high air content makes it suitable for use as a firewall.

The current study sought to gain new insights into the changes in ultrasonic pulse velocity (UPV), splitting tensile strength, modulus of elasticity, bending strength, compressive strength, thermal conductivity, porosity, and mass of FC when exposed to elevated temperatures (20 °C, 100 °C, 150 °C, 200 °C, 400 °C, 600 °C, and 800 °C). In addition, a slump test was used to determine the fresh properties of the mixtures. The morphology of pore size distribution, porosity hydration, and FC products were determined employing mercury intrusion porosimetry (MIP) and SEM techniques. FC with densities of 500 kg/m^3, 1000 kg/m^3, and 1500 kg/m^3 and mortar specimens with a density of 1980 kg/m^3 were produced to meet the goals of this investigation.

2. Novelty and significance of study

The mechanical durability, thermal characteristics, and microstructure of FC are influenced by factors that also affect its residual attributes at high temperatures, albeit showing different behaviours at ambient temperature. Variations in different high temperature levels, heating ratings, and times of exposure to fires have a major effect on the residual properties of FC. Evaluating the fire resistance of FC structures depends greatly on their ability to retain their properties during exposure to high temperatures.

After exposure to fire, the fire curve significantly contributes to the degradation of the mechanical, thermal, durability, and microstructural properties of FC. Various national standards, including ASTM E119, the hydrocarbon fire curve, DIN 4102, and ISO 834, are utilized to perform fire testing. The fire curves illustrate extreme unintended fire scenarios, especially in the underground and oil and gas sectors, while the ISO 834 fire curve replicates a typical commercial and residential fire. FC has become a popular choice for various applications in residential and commercial constructions, such as partitions, blocks, load-bearing panels, semi-load-bearing walls, and fire insulation materials. High temperatures will inevitably impact the use of FC in large-scale construction and infrastructure projects. Hence, it is essential to examine the functionality of FC according to ISO 834.

The mechanical, thermal, and durability properties of FC that were studied at elevated temperatures were found not to be according to the ISO 834 fire rating curve based on the literature. Additionally, the impact of temperature exposures and heating rates is subjective,

Table 1
Chemical compositions of OPC.

Oxide components	Percentage (%)
Calcium oxide (CaO)	66.94
Silicon dioxide (SiO_2)	14.02
Aluminium oxide (Al_2O_3)	3.97
Iron oxide (Fe_2O_3)	7.61
Magnesium oxide (MgO)	1.32
Sodium oxide (Na_2O)	0.29
Potassium oxide (K_2O)	0.89
Sulfur trioxide (SO_3)	4.96
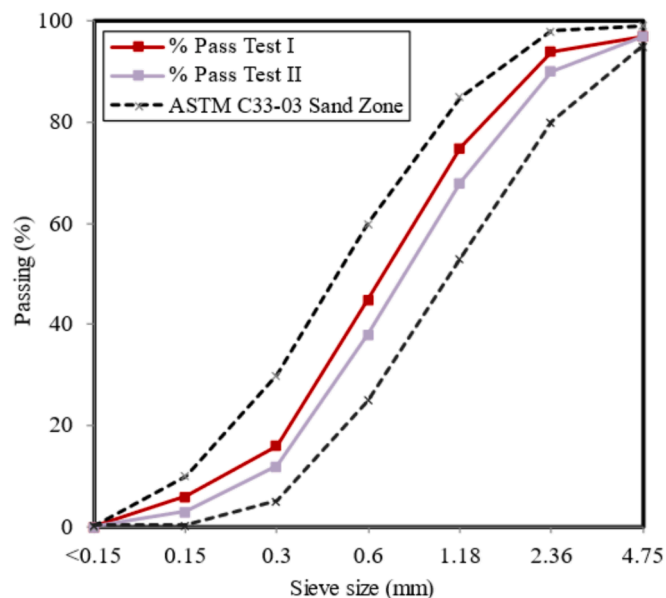
Fig. 1. Sieve analysis of aggregate following guidelines in ASTM C33-03 [37].

Table 2
Physical properties of OPC.

Components	OPC	Fine aggregate
Specific gravity	3.15	2.55
Apparent density (g/cm^3)	1440	1790
Moisture absorption (%)	3.19	2.25
Fineness modulus	–	2.35
Bulk porosity (%)	–	29

Table 3
Properties of foaming agent.

Properties	Description or Value
Appearance	Brown
Foam density (kg/m^3)	70 ± 5
Acidity (pH)	6.45
Specific gravity	1.10
Expansion ratio	15×
Suitable FC density (kg/m^3)	> 500

departing from previous studies' conventional fire cure ISO 834 recommendations. Research on the differences in the residual characteristics of FC with different densities after exposure to various high temperatures is lacking.

A detailed examination of the microstructural, mechanical, durability, and thermal properties of FC after exposure to various elevated temperatures is necessary to investigate its implications on its behaviour because there is an inadequate amount of data in the literature. Without

Table 4
Mix proportions of FC.

Mix reference	Target density (kg/m^3)	Wet density (kg/m^3)	Foam (kg/m^3)	Water (kg/m^3)	Aggregate (kg/m^3)	OPC (kg/m^3)
500-FC	500	619	46.29	95.4	286.3	190.9
1000-FC	1000	1136	30.66	184.2	552.7	368.4
1500-FC	1500	1653	15.03	273.0	819.0	546.0
1980-M	1980	2035	–	329.0	1073.0	715.3

Fig. 2. Portafoam PM-2 foam generator.

undertaking a thorough comparison, most earlier studies concentrated on the specific density of FC. In this study, mortar (without foam) weighing 1980 kg/m^3 was compared to FC with low, medium, and high densities (500 kg/m^3, 1000 kg/m^3, and 1500 kg/m^3). This study's originality lies in its ability to provide material scientists and product developers with a better grasp of the various densities of FC that respond to different elevated temperatures. Hence, they could develop an excellent FC-based product to be used for fire-resistant purposes.

3. Experimental program

3.1. Materials

The main components of FC are foaming agent, water, fine aggregate, and OPC. The OPC grade was CEM I 52.5 N, which met BS EN 197–1 [36] specifications. Table 1 outlines the chemical compositions of OPC. Natural sand was utilized as fine aggregate from a local supplier. According to ASTM C 33–03 [37], the findings of the sieve analysis are presented in Fig. 1. Table 2 lists the physical characteristics of OPC and fine aggregate. In accordance with BS-3148 [38], water used in the investigation had an average temperature of 20 ± 2 °C.

Foam solutions were made by diluting a protein-based foaming agent (Noraite PA-1) with a 1:30 ratio of water to achieve a 70 kg/m^3 density. The characteristics of the protein-based foaming agent used in this study are shown in Table 3.

Fig. 3. Quantity of foam was measured and subsequently incorporated into cement slurry.

Fig. 4. Freshly prepared FC mixture was placed into steel moulds.

(a)   (b)
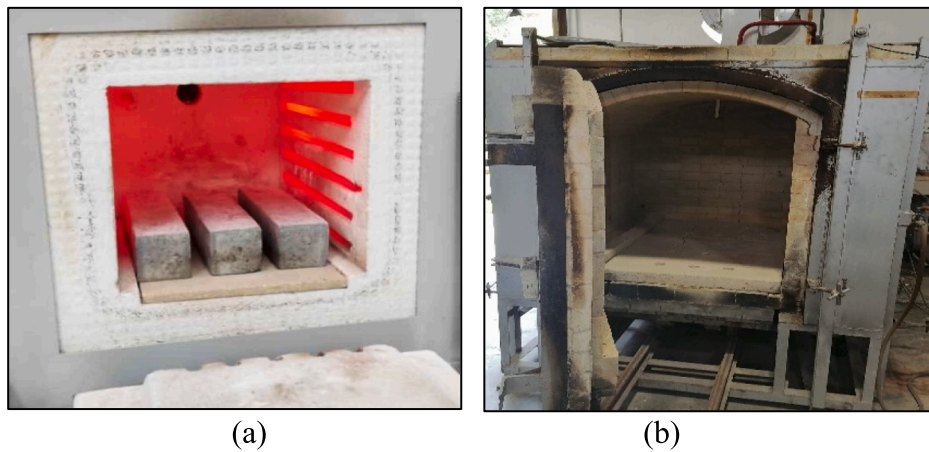
Fig. 5. Heat treatment for elevated temperature testing: (a) electric furnace; (b) gas furnace.

3.2. Mix proportions

A comprehensive set of four mixtures was formulated, comprising three compositions of FC and one composition of mortar. The target densities of FC were 500 kg/m³, 1000 kg/m³, and 1500 kg/m³. The density of mortar was measured to be 1980 kg/m³. The three densities of FC were chosen because of the use of low-density FC (500 kg/m³) as non-load bearing elements, infill materials, and partition blocks. A medium density of 1000 kg/m³ is used for semi-load-bearing elements in building construction as well as for low-rise buildings. While high density (1500 kg/m³) is utilized for load-bearing elements in building construction. As a result, it is critical to understand exactly how high, medium, and low densities of FC react to high temperatures. The mixture was prepared with a ratio of 1:1.5:0.45 (cement, aggregate, and water). In this study, low, medium, and high densities of FC were considered to compare the proportion of deterioration upon exposure to
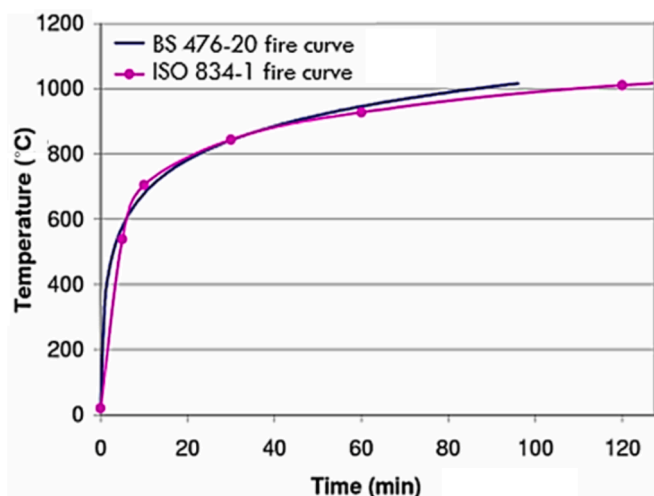
Fig. 6. Standard fire curve in accordance with ISO 834 and BS 476.

elevated temperatures. The quantity of water directly influences the consistency and stability of FC. As a result, it was critical to adjust the amount of water in the mix to maintain its spreadability within the 250 ± 15 mm range. Table 4 presents the FC's mix proportions utilized in the various mixtures considered within the scope of this study.

3.3. Production of FC

The main components necessary to produce FC include OPC, fine aggregate, clean water, and a stable foam. Initially, a drum mixer was employed to incorporate fine aggregate, which was subsequently blended with 20% of the predetermined water quantity. Subsequently, OPC was added to the mixture. To achieve uniformity, the constituents were allowed to remain in the mixer for approximately three minutes. Then, the remaining water was incrementally incorporated until the desired consistency of mortar was achieved. Next, a predetermined quantity of foam generated by the Portafoam TM-2 system, as demonstrated in Fig. 2, was incorporated into the base mixture to attain the desired density, as illustrated in Fig. 3. The density of FC was measured promptly following the complete blending of the foam. The consistency of freshly mixed FC was found to be homogeneous, with no signs of segregation or bleeding, as indicated by the ratio of the fresh density to the designated density. Next, the FC mixture was placed into steel moulds, as shown in Fig. 4. A plastic sheet was positioned on top of the moulds for a duration of 24 h. Subsequently, the FC specimens were extracted from their moulds and securely enclosed for a duration of 28 days to undergo the curing process. In this study, a moisture curing regime was used. Following this, the specimens were subjected to oven-drying at 105 °C to ensure that all moisture was eliminated, and the specimens achieved a constant weight prior to testing. This was carried out to make sure that all pores connecting to the surface of the FC specimens were empty and entirely absorbent.

3.4. Heating of samples at elevated temperatures

To facilitate the evaluation of the mechanical properties in the current study, an unstressed test method was implemented. In the unstressed test, the samples were heated at a constant rate to the predetermined temperature without the application of any burden throughout the heating procedure. Four distinct subgroups of the specimens were subjected to temperatures that were predetermined to be 200 °C, 400 °C, 600 °C, and 800 °C. The electrical furnace, depicted in Fig. 5(a) and with the dimensions 750 × 750 × 750 mm, was utilized to attain pre-determined temperatures reaching 400 °C. A gas furnace with a built-up area of 800 × 2000 × 1500 mm was used. Thermal exposure

profiles are produced by programmable microprocessor temperature controllers that are connected to the power supply of both gas and electric furnaces. The temperature within the furnace chamber was monitored by a Type K thermocouple. Temperatures in both furnaces were regulated in accordance with ISO 834 [39] so that their relationship with time resembled that of a standard fire curve. The standard fire curve of ISO 834 is compared to that of BS 476 in Fig. 6. After subjecting all the FC specimens to the predetermined target temperature during the heating procedure, they were maintained at that temperature for one hour, as suggested by Kodur et al. [40]. Following that, the specimens were placed in the furnace to undergo a cooling process for a period of 24 h before the intended evaluations were carried out.

3.5. Testing methods

To examine the workability of the FC samples with varying densities, a flow table test was conducted, as displayed in Fig. 7(a). The freshly generated FC mixtures were placed in an open-ended cylindrical container with dimensions of 76.2 mm in diameter and 152.4 mm in height. The cylinder was then raised to allow the FC mixtures to flow freely. Measurements were conducted to determine the spread widths in both directions, and subsequently, an average value was determined. To ascertain the mass reduction of FC at various predetermined temperatures, measurements were done to establish the dry density of FC both prior and after subjecting it to specific elevated temperatures.

The permeable porosity of FC was determined using a vacuum saturation apparatus, as demonstrated in Fig. 7(b). The test employed cylindrical specimens with a diameter of 45 mm and a height of 50 mm. To remove moisture from the specimens, they were placed in an oven for 72 h or until no weight changes were recorded. Afterwards, each specimen was cooled, and its weight was recorded as W_{dry}. In a vacuum desiccator, the specimens were immersed for 72 h or until bubbles could not be seen. The specimens' weights were recorded in water, W_{wet}, and in air, W_{dry}. To calculate the FC's permeable porosity, equation (1) was utilized.

$$Permeable\ porosity\ (\%) = \frac{W_{sat} - W_{dry}}{W_{sat} - W_{wet}} \times 100\% \qquad (1)$$

where;

W_{sat} = saturated surface dry weight of FC specimen (kg).
W_{dry} = oven dried weight of FC specimen (kg).
W_{wet} = weight of FC specimen in water (kg).

Next, the pore size distributions of the FC mixtures were determined using MIP. This method provides quick information about the pores' structures. The pore diameter can be measured by MIP, which varies from 0.001 μm to 1000 μm based on the injection pressure.

A compression test was performed on the cube specimens with dimensions of 100 mm, and their compressive strength was assessed at 28 days. The cube specimens were subjected to a 0.5 MPa/sec loading rate, following the guidelines outlined in BS-EN-12390–3 [41]. Fig. 7(c) illustrates the configuration employed for conducting the compression tests. The bending strength of the prisms measuring 100 × 100 × 500 mm was evaluated at the 28-day curing age, in accordance with the specifications outlined in BS-EN-12390–5 [42]. The specimens of the prism were subjected to loading at a rate of 0.3 MPa per second using a three-point bending test setup, as indicated in Fig. 7(d). The split tensile strength test was done in accordance with the specifications mentioned in BS12390-6 [43]. The experiment was carried out at the curing age of 28 days. Cylindrical specimens with a diameter of 100 mm and a height of 200 mm, as depicted in Fig. 7(e), were utilized for the test. Next, the modulus of elasticity of FC was determined by adhering to ASTM C469 [44], employing 100 × 200 mm cylinders and conducting the test at the 28-day curing age. The thermal conductivity test was executed using the hot guarded plate (HGP) method, following the guidelines in ASTM C177 [45]. The experimental configuration is shown in Fig. 7(f). The
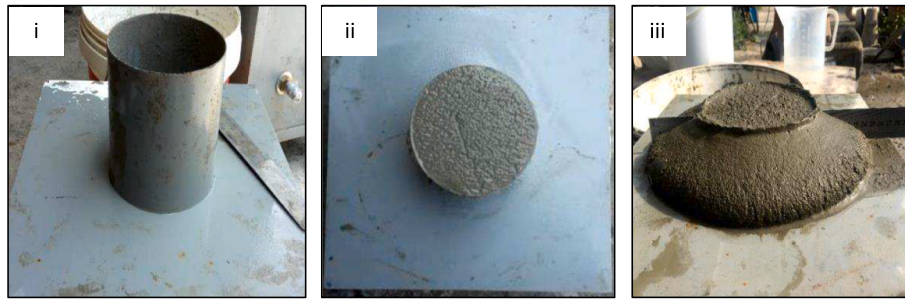
(a) flow table test; (i) open ended cylinder container, (ii) fresh mix was poured to fill container, (iii) mould was removed and spread diameter was measured using a ruler

(b) permeable porosity test   (c) axial compression test
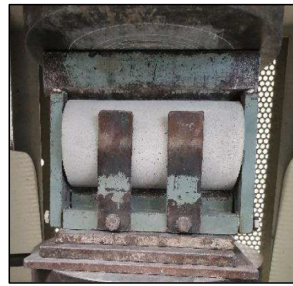
(d) three-point bending test   (e) split tensile strength test   (f) thermal conductivity test

(g) UPV test

Fig. 7. Testing organisations and setups.

measurement of UPV was done in accordance with the specifications in BS12504-4 [46]. The experimental procedure involved utilizing the direct transmission technique to determine the velocity of ultrasonic waves in a prism measuring $100 \times 100 \times 500$ mm, as displayed in Fig. 7 (g).

4. Results and discussion

4.1. Slump flow

Fig. 8 indicates the slump flow results for the fresh FC mixtures with densities of 500 kg/m^3, 1000 kg/m^3, and 1500 kg/m^3 and mortar with density of 1980 kg/m^3. Based on Fig. 8, the slump flow value of the examined FC samples diminished progressively as the density rose, with

the maximum slump flow value occurring at 500 kg/m^3. The finding can be explained by two factors: (1) the larger quantity of water generated by foam led to fewer solid constituents per unit volume of FC and (2) the round-shaped foam within the binding matrix was able to decrease frictions between various constituents of the binder, thereby enhancing the overall fluidity of the fluid phase. Employing FC with densities of 1000 kg/m^3 and 1500 kg/m^3 reduced the slump flow value by 3.14% and 5.09%, respectively, in comparison to FC with a density of 500 kg/m^3. Nevertheless, the greatest reduction in the slump flow value was 7.45% for mortar with a density of 1980 kg/m^3. This can be owing to the increase in demand for water due to the mortar's increased solid content [47].
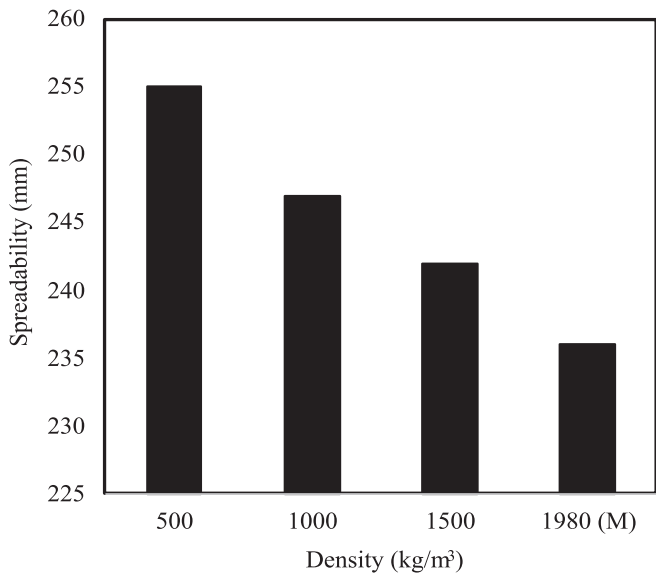
Fig. 8. Influence of varying densities on slump flow diameter of FC.

4.2. Appearance and colour changes

At elevated temperatures, spalling and cracks are considered reliable indicators for the degree of the concrete damage. In general, the degradation in the appearance of concrete is triggered by internal stresses that form at elevated temperatures because of the chemical transition, drying shrinkage, thermal expansion, and water evaporation [48–50]. The FC's appearance with densities of 500 kg/m^3, 1000 kg/m^3, and 1500 kg/m^3 and mortar samples with a density of 1980 kg/m^3 at ambient temperature (20 °C) as well as at elevated temperatures (200 °C, 400 °C, 600 °C, and 800 °C) are illustrated in Figs. 9–12. At room temperature, raising the density to 1500 kg/m^3 formed a little darker surface due to the high absorption and the dark colour of cement with rising quantities of aggregate and reducing quantities of foam agent. Since the samples with a 1980 kg/m^3 density contained a greater quantity of cement, there was no alteration in colour owing to their dense microstructure, which prevented the internal water pressure from being easily released. When the samples were subjected to heating at 200 °C, the appearance of all the mixtures up to 1500 kg/m^3 did not alter significantly. As a consequence of the chemical transformations, a lighter colour and pore connectivity can be detected at elevated temperatures [51]. With the exception of mortar with a density of 1980 kg/m^3, all the mixtures at 400 °C exhibited merged pores that became greater with the density contents. At 600 °C, obvious cracks appeared in all the mixtures, and spalling occurred in the samples with densities of 500 kg/m^3, 1000 kg/m^3, and 1500 kg/m^3. After being exposed to 800 °C, the cracks grew longer and wider, and the severity of the pore connectivity and spalling increased considerably. Generally, a rise in the density enhances the FC's appearance by reducing merged pores, spalling, and cracks. Furthermore, the development of cracks at 600 °C and 800 °C indicated that the compressive strength and material's density would be substantially diminished. As low-density mixtures (500 kg/m^3 and 1000 kg/m^3) showed the greatest spalling, rough edges were

| (a) ambient | (b) 200°C | (c) 400°C | (d) 600°C | (e) 800°C |
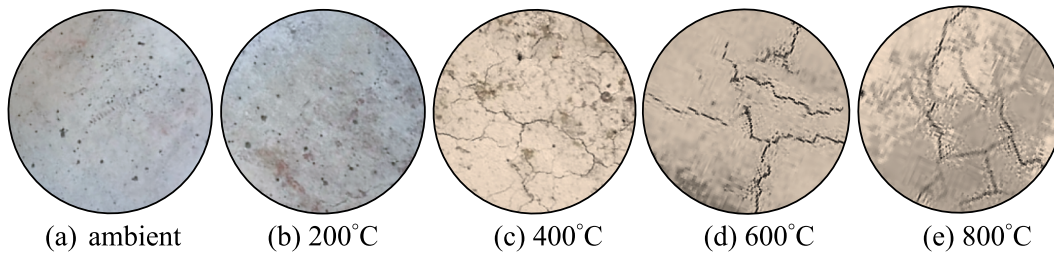
Fig. 9. Appearance and colour changes of FC specimens with a density of 500 kg/m^3 at specific predetermined temperatures.

| (a) ambient | (b) 200°C | (c) 400°C | (d) 600°C | (e) 800°C |
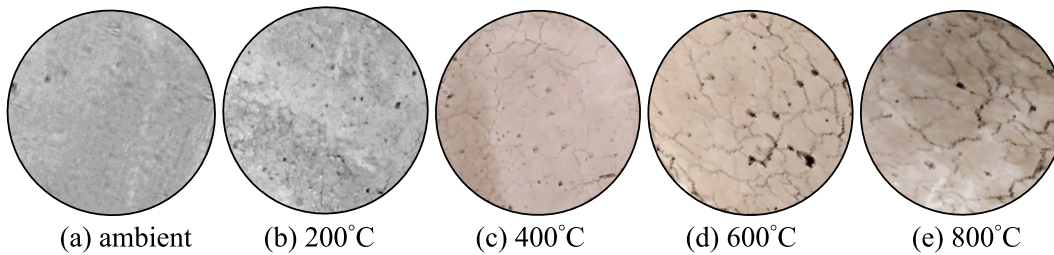
Fig. 10. Appearance and colour changes of FC specimens with a density of 1000 kg/m^3 at specific predetermined temperatures.

| (a) ambient | (b) 200°C | (c) 400°C | (d) 600°C | (e) 800°C |
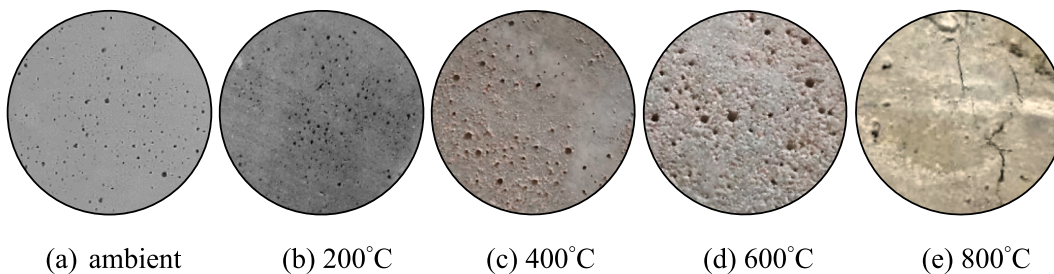
Fig. 11. Appearance and colour changes of FC specimens with a density of 1500 kg/m^3 at specific predetermined temperatures.

(a) ambient   (b) 200°C   (c) 400°C   (d) 600 °C   (e) 800°C
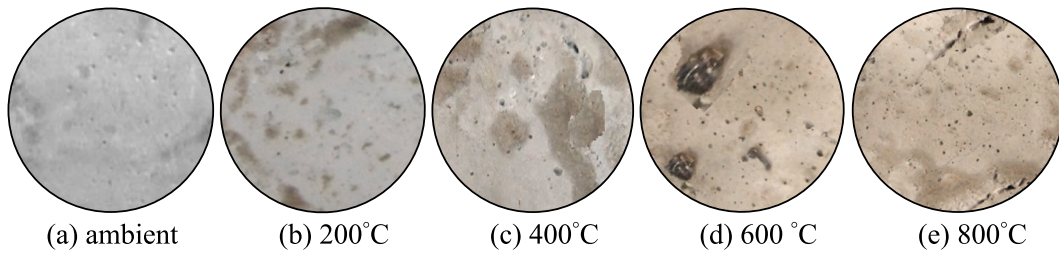
Fig. 12. Appearance and colour changes of mortar specimens with a density of 1980 kg/m³ at specific predetermined temperatures.
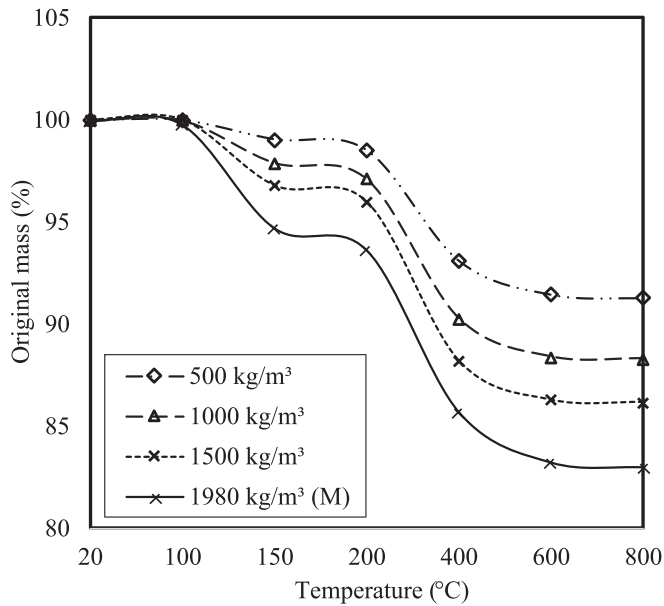
Fig. 13. Mass loss for FC samples with three densities and mortar samples with one density exposed to high temperatures.
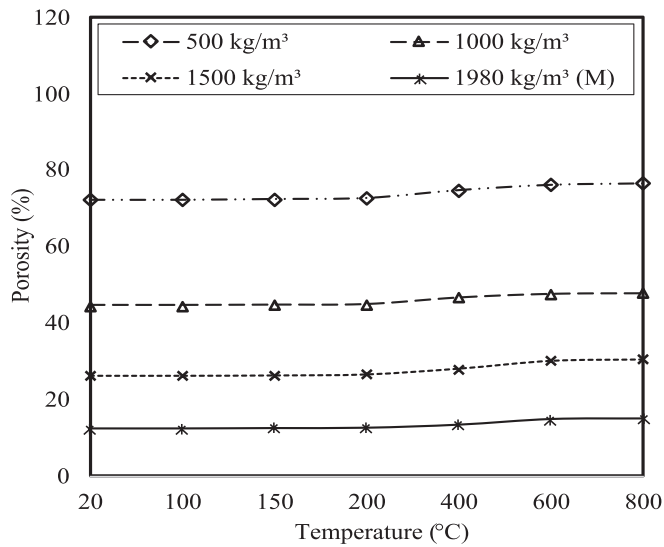
Fig. 14. Porosity for FC samples with three densities and mortar samples with one density exposed to high temperatures.
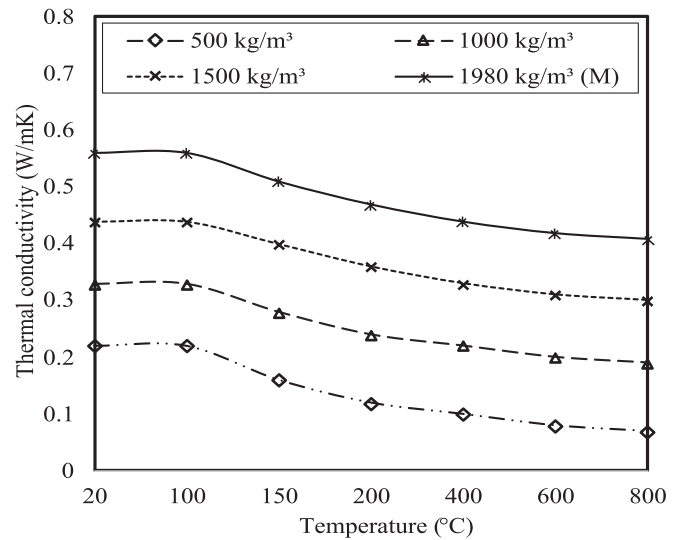
Fig. 15. Thermal conductivity for FC samples with three densities and mortar samples with one density exposed to high temperatures.
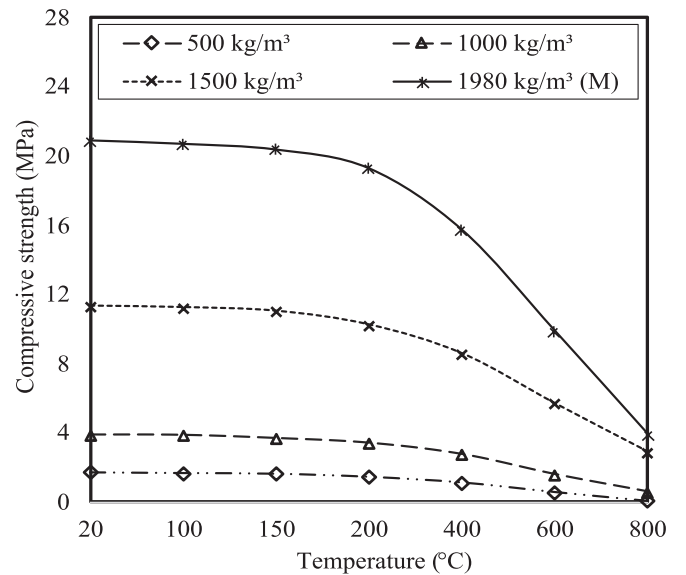
Fig. 16. Compressive strength for FC samples with three densities and mortar samples with one density exposed to high temperatures.

noticed at 600 °C and 800 °C.

4.3. Mass loss

At elevated temperatures, the mass loss is a crucial factor because it
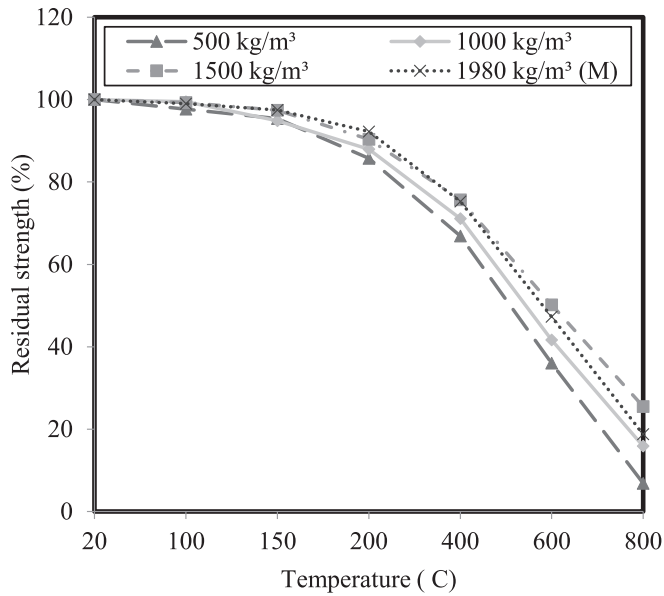
Fig. 17. Residual compressive strength for FC samples with three densities and mortar samples with one density exposed to high temperatures.
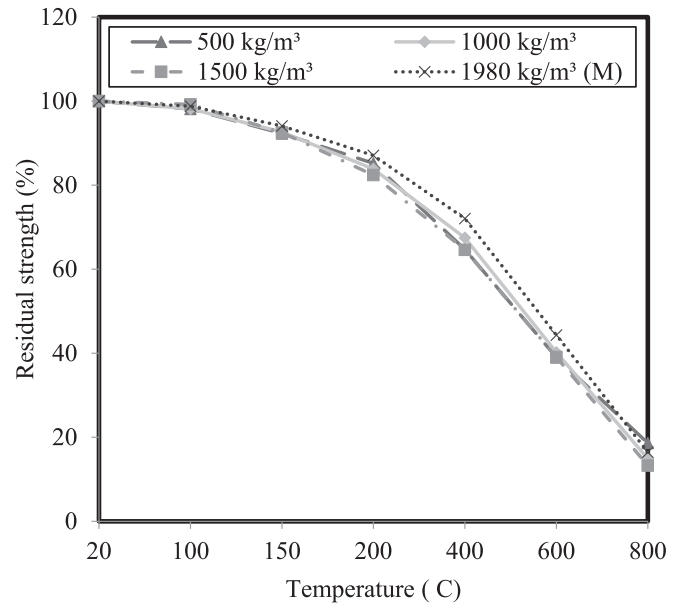
Fig. 19. Residual bending strength for FC samples with three densities and mortar samples with one density exposed to high temperatures.
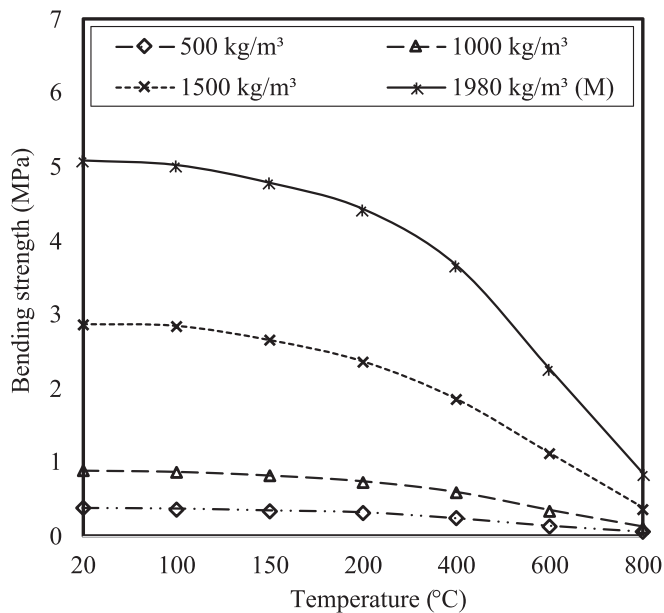
Fig. 18. Bending strength for FC samples with three densities and mortar samples with one density exposed to high temperatures.
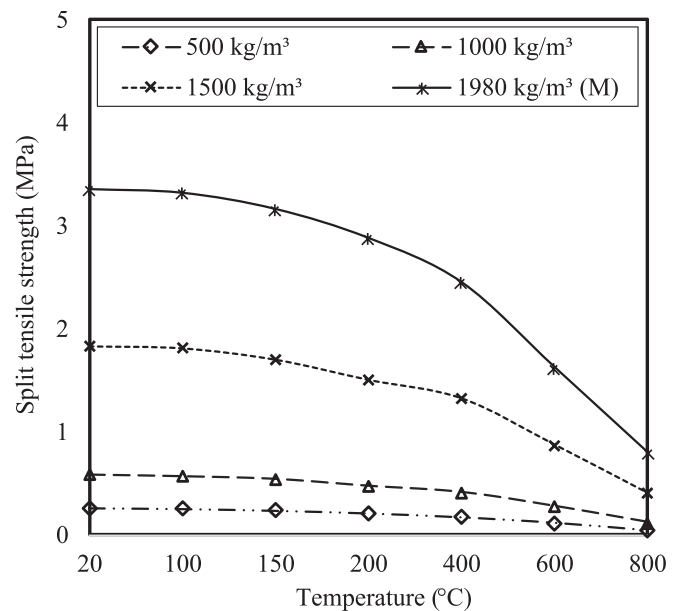
Fig. 20. Split tensile strength for FC samples with three densities and mortar samples with one density exposed to high temperatures.

eliminates various forms of moisture within the matrix, including capillary water, interlayer water, absorbed, adsorbed, and free. To determine the mass loss of all the specimens, the mass ratio at the target temperature to the mass ratio at ambient conditions was calculated. Fig. 13 depicts the percentages of the mass loss for the mortar specimens and FC, when subjected to higher temperatures. The FC's mass loss reduced progressively when the temperature rose, whereas the previous pattern was nearly the same across all the mixtures.

The reduction was caused by physically absorbed water and capillary water loss at temperatures as high as 400 °C [48]. The Ca(OH)$_2$ dehydration induced the mass loss at greater temperatures because of the loss of the chemically bound water [52]. In addition, the difference in the mass loss between 400 °C and 200 °C was comparatively low since the free water entirely evaporated between 100 °C and 200 °C [53]. As

demonstrated in Fig. 12, the samples with a density of 1980 kg/m^3 experienced greater mass loss, as increasing the concrete density leads to greater mass loss, with the increase in the mass loss becoming more obvious at 800 °C and 600 °C. The rise in the mass loss could be explained by the rise in the solid content subjected to high temperatures when the density increased. Similar findings were recorded as the FC's density increased for the rise within the solid matrix [25,54,55].

Obviously, different ratios were witnessed for the temperature and density. The results illustrated values of 0.93%, 1.47%, 6.87%, 8.52%, and 8.7% at 150 °C, 200 °C, 400 °C, 600 °C, and 800 °C, respectively, compared to the control (at 20 °C) for FC with a density of 500 kg/m^3. While the results indicated values of 2.08%, 2.88%, 9.73%, 11.6%, and 11.69%, respectively, for FC with a density of 1000 kg/m^3. For FC with a density of 1500 kg/m^3, the values were 3.21%, 4.01%, 11.79%, 13.69%,
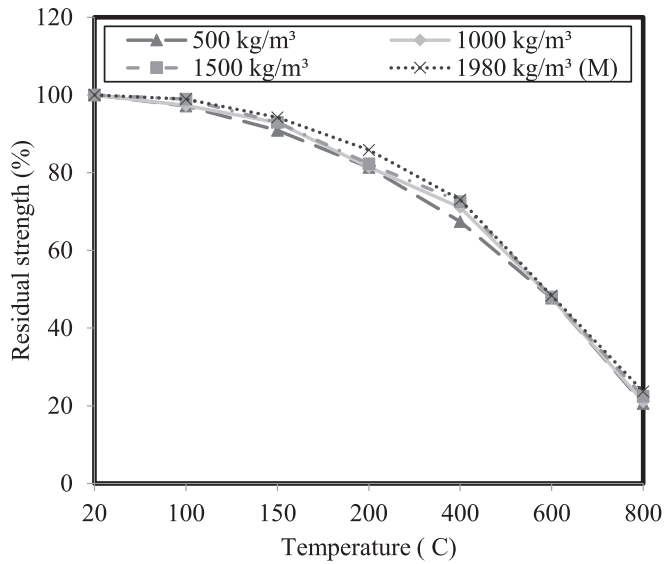
Fig. 21. Residual split tensile strength for FC samples with three densities and mortar samples with one density exposed to high temperatures.
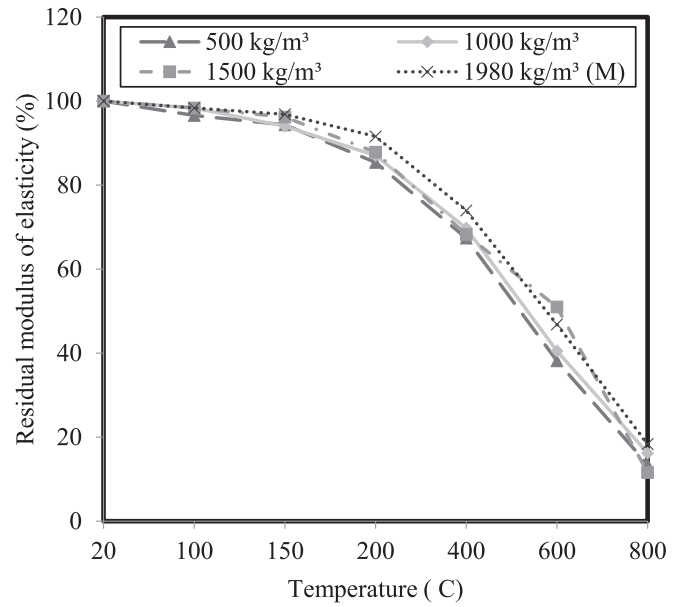
Fig. 23. Residual modulus of elasticity for FC samples with three densities and mortar samples with one density exposed to high temperatures.

Fig. 22. Modulus of elasticity for FC samples with three densities and mortar samples with one density exposed to high temperatures.
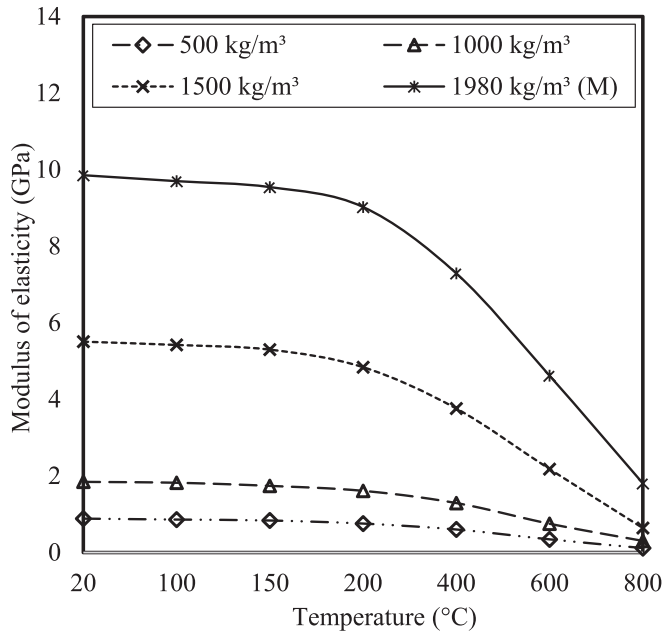
Fig. 24. UPV values for FC samples with three densities and mortar samples with one density exposed to high temperatures.

and 13.8%, respectively. The results exhibited values of 5.27%, 6.35%, 14.29%, 16.75%, and 16.98%, respectively, for mortar with a density of 1980 kg/m³. Similarly, Sayadi [56] reported that FC with lower densities showed worse fire resistance in comparison to FC with higher densities after comparing 450 kg/m³, 250 kg/m³, and 150 kg/m³.

4.4. Porosity

The porosity tests' results for the FC samples with densities of 500 kg/m³, 1000 kg/m³, and 1500 kg/m³ and mortar samples with a density of 1980 kg/m³ are illustrated in Fig. 14. The samples were heated to 20 °C, 100 °C, 150 °C, 200 °C, 400 °C, 600 °C, and 800 °C. As depicted in Fig. 14, the porosity of FC increased with increasing the temperature, and the mixtures with a density of 500 kg/m³ had the maximum values

of the porosity. The FC's porosity increased uniformly throughout all three densities, but at a slower rate with a density of 1980 kg/m³. The initial porosity values for densities of 500 kg/m³, 1000 kg/m³, 1500 kg/m³, and 1980 kg/m³ were 72.844%, 45%, 26.72%, and 12.88%, respectively. Ranging from 200 °C to 400 °C, the porosity of FC for higher densities rose noticeably.

As different amounts of sulfoaluminate and calcium silicate hydrate gel broke down, the rise was less considerable for the lower-density FC. However, the porosity of the lower-density FC (500 kg/m³) increased significantly. On the other hand, the rise was less noticeable for the higher-density FC samples (1500 kg/m³ and 1000 kg/m³) and mortar samples (1980 kg/m³). For 400 °C, the measured porosity values of the samples with densities of 500 kg/m³, 1000 kg/m³, 1500 kg/m³, and 1980 kg/m³ were 74.97%, 46.82%, 28.25%, and 13.6%, respectively. At temperature of 400 °C, the measured porosity increased because of the

(a) 20ºC   (b) 400ºC   (c) 800ºC
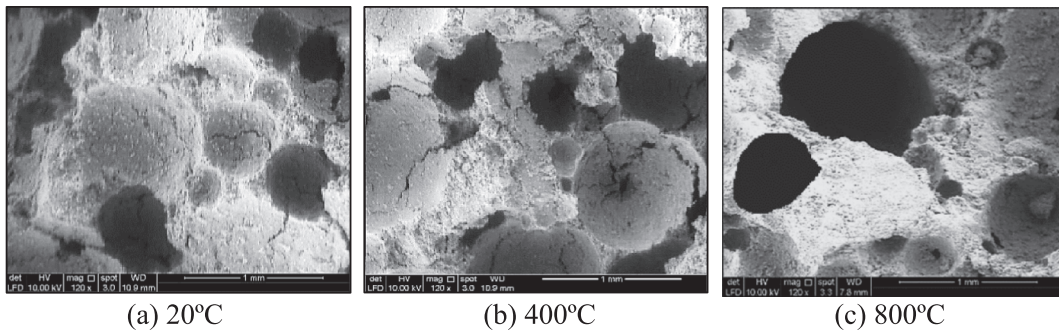
Fig. 25. SEM images of FC with a density of 500 kg/m^3 exposed to various temperatures.

(a) 20ºC   (b) 400ºC   (c) 800ºC
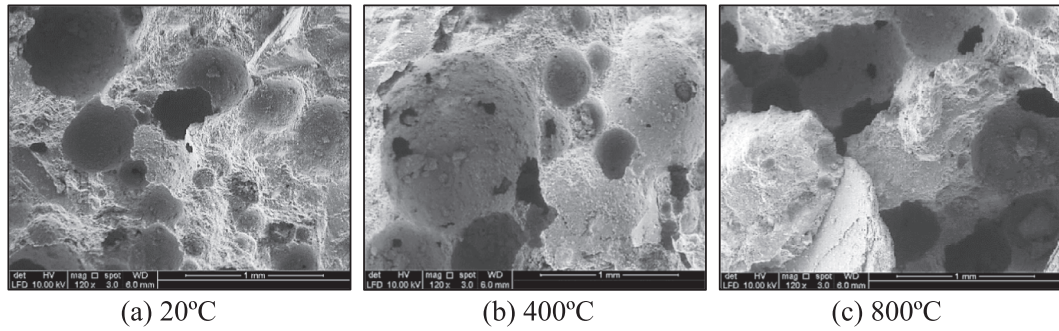
Fig. 26. SEM images of FC with a density of 1000 kg/m^3 exposed to various temperatures.

(a) 20ºC   (b) 400ºC   (c) 800ºC
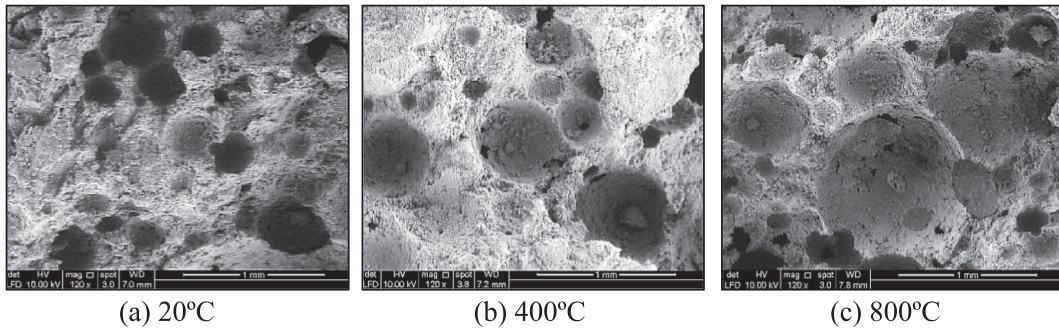
Fig. 27. SEM images of FC with a density of 1500 kg/m^3 exposed to various temperatures.

(a) 20ºC   (b) 400ºC   (c) 800ºC
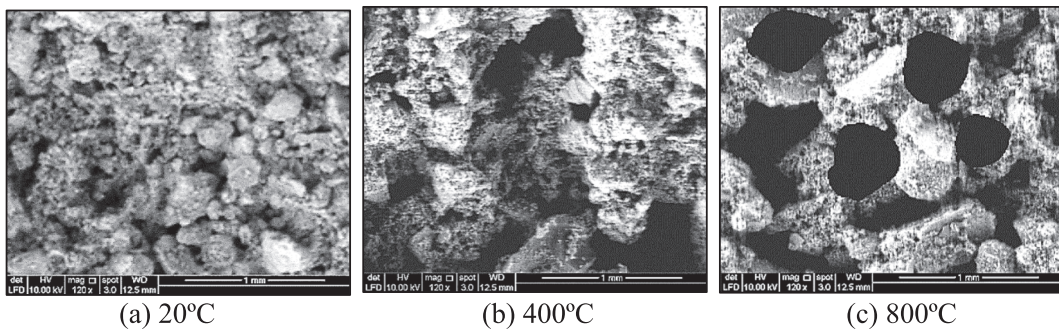
Fig. 28. SEM images of mortar with a density of 1980 kg/m^3 exposed to various temperatures.

calcium hydroxide decomposition into calcium oxide. For 600 °C, the porosity values of the samples with densities of 500 kg/m^3, 1000 kg/m^3, 1500 kg/m^3, and 1980 kg/m^3 were 76.41%, 47.82%, 30.31%, and 15.09%, respectively. Because of the large porosity at room temperature, mortar and FC might be recognised as possessing a fixed porosity at

various temperatures.

4.5. Thermal conductivity

Fig. 15 demonstrates the thermal conductivity of the FC samples with
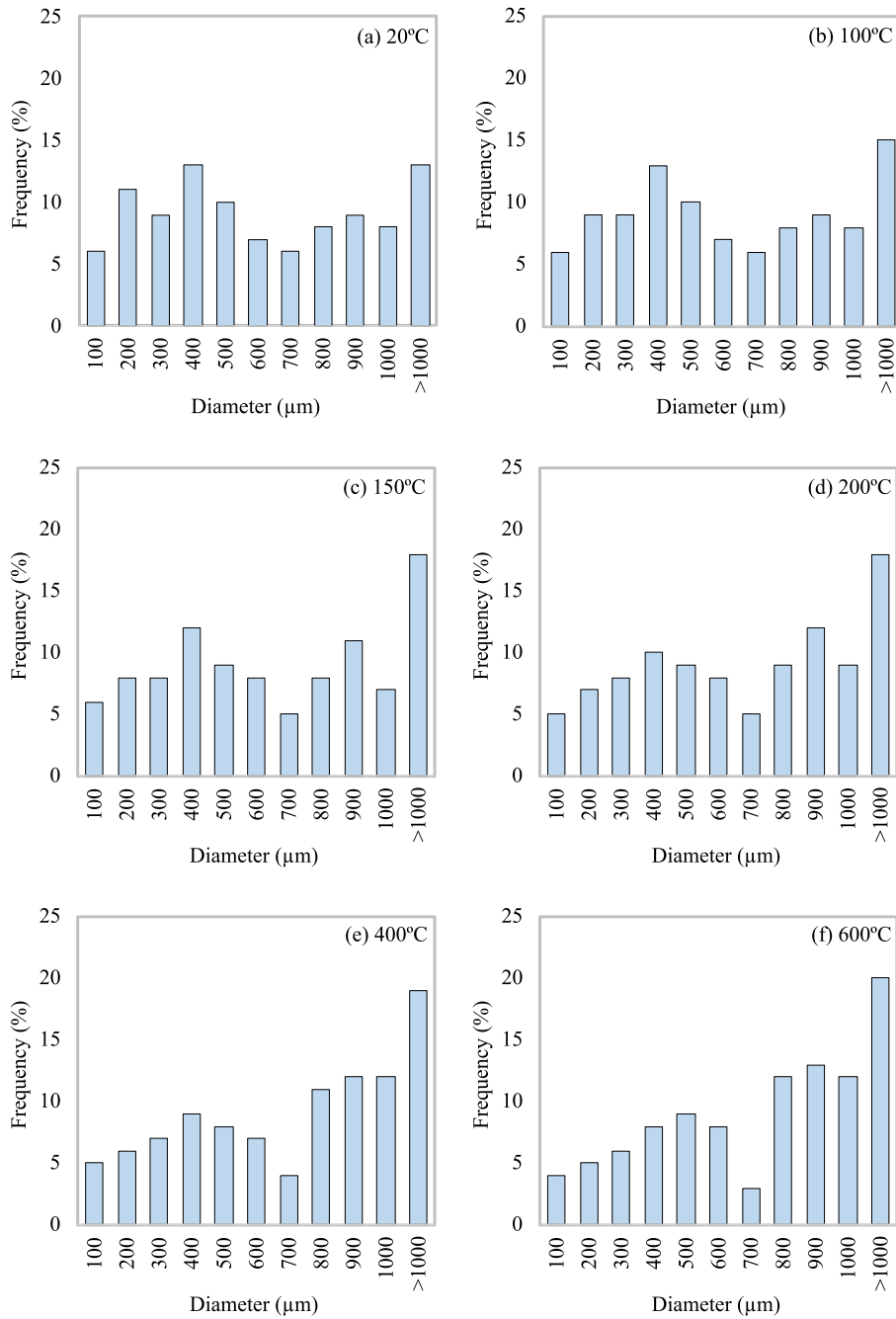
Fig. 29. Pore size distribution of FC specimens with a density of 500 kg/m³ exposed to various temperatures.

densities of 500 kg/m³, 1000 kg/m³, and 1500 kg/m³ and mortar samples with a density of 1980 kg/m³ after being exposed to high temperatures (20 °C, 100 °C, 150 °C, 200 °C, 400 °C, 600 °C, and 800 °C). The thermal conductivity of the mortar and FC samples decreased with temperature for all the densities considered in this study, as displayed in Fig. 15. The samples with a high content of cement exhibited a high thermal conductivity coefficient at room temperature. As the volume of foam in the mix increased, the value declined. As a result of its closed cellular structure, FC that had limited thermal conductivity indicated a favourable thermal performance. As the thermal conductivity is associated with density, which is heavily reliant on the pore structure and porosity [57], the thermal conductivity declining pattern with rising temperatures can be ascribed to a rise in the volume of the permeable voids. Previous investigations [58–60] have also

documented this behaviour. After exposure to high temperatures, the values of the thermal conductivity for the FC samples were lower in comparison to the values at ambient temperature.

As soon as the dry unit weight and porosity are considered together, the decrease in the thermal conductivity after elevated temperatures confirms this point. At 250 °C, Othuman and Wang [29] found that the thermal conductivity of FC with a density of 650 kg/m³ decreased from 0.226 W/mK at room temperature to 0.144 W/mK. At 250 °C, the thermal conductivity of FC with a density of 1000 kg/m³ reduced from 0.309 W/mK at room temperature to 0.245 W/mK. The thermal conductivity of FC with a density of 1850 kg/m³ decreased from 0.484 W/mK at room temperature to 0.434 W/mK after 250 °C. It appears that such results match the findings of this investigation.
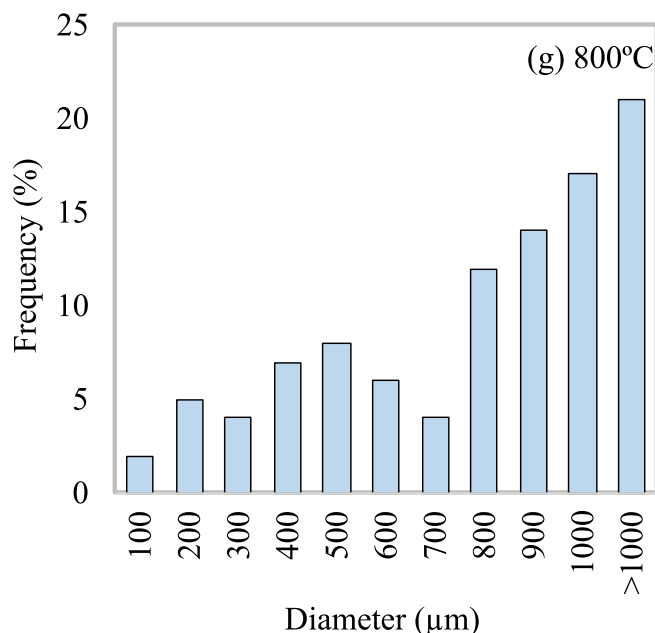
Fig. 29. (*continued*).

4.6. Compressive strength

At elevated temperatures, the compressive strength degrades due to the chemical composition and structural changes. The concrete hydration products, including C-S-H, ettringite, and portlandite, undergo the phase transformation, resulting in the formation of active materials such as calcium silicate and lime [61,62]. Figs. 16 and 17 show the FC samples' compressive strength and residual compressive strength with different densities (500 kg/m^3, 1000 kg/m^3, and 1500 kg/m^3), as well as those of the mortar samples (1980 kg/m^3), respectively, after being exposed to high temperatures. The FC's compressive strength increased progressively employing higher densities after exposure to high temperatures, as illustrated in Fig. 16. In comparison to the sample with a density of 500 kg/m^3, the compressive strength of the samples with densities of 1000 kg/m^3, 1500 kg/m^3, and 1980 kg/m^3 increased by 123.42%, 548%, and 1,097.14%, respectively, at 20 °C. The rise was a result of the continuous development of the microstructure of concrete, which increased the solid matrix as it grew in the density.

However, the results demonstrated that the compressive strength of all the mixtures decreased after being exposed to temperatures ranging from 20 °C to 800 °C. Because the temperature range of 100 °C to 200 °C had a minor impact on the strength of mortar and FC, all the samples retained at least 95% of their capacity. Similar findings were found in previous research works at the same temperatures [33,48,62]. During this phase, FC lost the strength due to the moisture loss, which caused the paste to shrink and generate microcracks. As the temperature rose from 90 °C to 180 °C, the strength subjected to compression progressively decreased because of the release of the chemically bound water and free water.

The decrease in the compressive strength at temperatures ranging from 25 °C to 160 °C was similar to a reduction in Van der Waals forces cohesiveness (molecular interactions or distance-dependent interatomic) between the C-S-H layers. This decreased the surface energy of C-S-H, leading to the formation of silanol bands, accompanied by a decrease in the overall bonding strength.

In addition, the residual compressive strength of each mix decreased significantly as the temperature exceeded 200 °C. At 400 °C, the residual compressive strengths of the mixtures with densities of 500 kg/m^3, 1000 kg/m^3, 1500 kg/m^3, and 1980 kg/m^3 were 66.85%, 71.1%, 75.66%, and 75.27%, respectively, of those in ambient temperature. At these temperatures, the cementitious materials' decomposition resulted in the formation of microcracks, which remarkably affected the FC's compressive strength [33]. At 600 °C, the FC's residual compressive strengths with densities of 500 kg/m^3, 1000 kg/m^3, 1500 kg/m^3, and 1980 kg/m^3 were reduced to 36%, 41.68%, 50.17%, and 47.3%, respectively, compared to those in ambient temperature. Moreover, raising the density improved the residual compressive strength values at 400 °C and 600 °C by a small amount. In addition, the different densities' impact was more pronounced at 800 °C, in which reductions of 6.85%, 15.85%, 25.48%, and 18.75% were recorded for densities of 500 kg/m^3, 1000 kg/m^3, 1500 kg/m^3, and 1980 kg/m^3, respectively, compared to those in ambient temperature. Therefore, the minor decrease in the compressive strength with rising density is primarily attributable to the improvement of the microstructure by the gradual increase of the solid matrix (Figs. 16 and 17). The mortar mix with a density of 1980 kg/m^3 exhibited a slight decrease in the residual compressive strength compared to the samples with a density of 1500 kg/m^3 when exposed to temperatures exceeding 400 °C. The marginal reduction in the residual compressive strength was due to the expansion of the solid volume subjected to heat as the cement content rose in the mortar specimens. As the amount of Ca(OH)$_2$ in the mortar specimens increased, it began to breakdown beyond 400 °C, leading to a drop in the strength.

4.7. Bending strength

The bending test was designed to determine the strength during bending of mortar and FC, as brittle materials. The differences in the bending strengths and residual bending strengths of the mortar and FC samples as a function of temperatures are depicted in Figs. 18 and 19, respectively. The FC samples' bending strengths decreased significantly after 90 °C, disregarding the FC's density. Compatible with alterations to the other previously mentioned FC's mechanical characteristics, this illustrates that microcracking, which appears as free water and chemically bound water released from the porous body, is the main mechanism producing degradation.

The FC's chemical composition began to deteriorate between 200 °C and 300 °C due to the decomposition of the sulfoaluminate process (3CaO-Al$_2$O$_3$-CaSO$_4$-12H$_2$O and 3CaO-Al$_2$O$_3$-3CaSO$_4$-31H$_2$O) and C-S-H, resulting in the development of cracks and a considerable drop in the
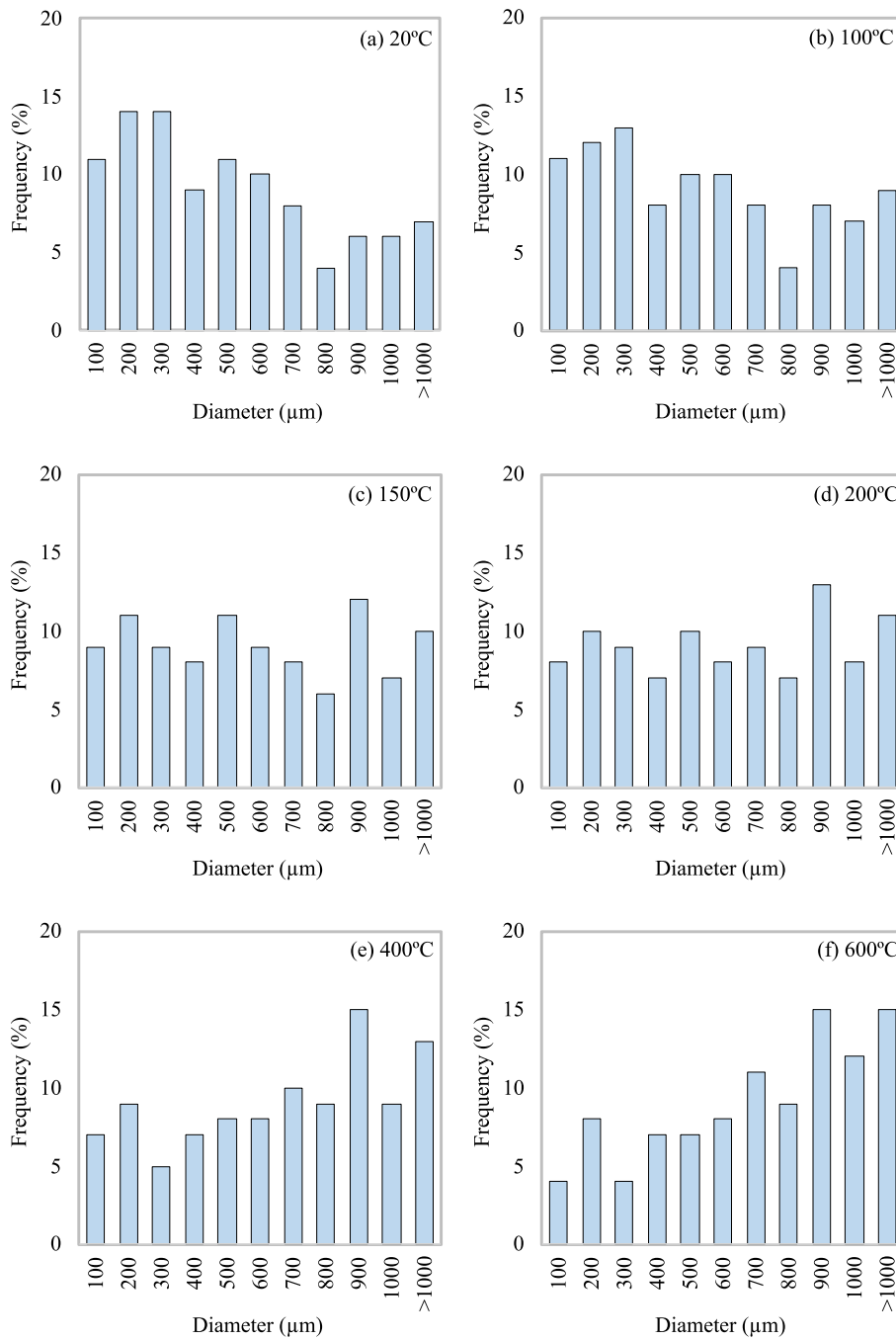
Fig. 30. Pore size distribution of FC specimens with a density of 1000 kg/m^3 exposed to various temperatures.

strength. At 400 °C, the bending strengths in all densities decreased to around 64% to 72% compared to those in ambient temperature. At 800 °C, the bending strength values were as follows: 18.62% for a density of 500 kg/m^3, 14.92% for a density of 1000 kg/m^3, 13.28% for a density of 1500 kg/m^3, and 16.48% for a density of 1980 kg/m^3. The noticeable decrease in the bending strength between 400 °C and 800 °C can be attributed to the development of extensive cracks. The evaporation of both chemically bound and free water caused internal shrinkage, which decreased the binding between the cementitious matrix and FC fine filler. After undergoing the same heat treatment, the mix's compressive strength is significantly higher than its bending strength.

4.8. Split tensile strength

The results of the split tensile strength experiments at different temperatures are depicted in Fig. 20. Fig. 21 shows a comparison of the residual split tensile strengths of different mixtures. The split tensile strength followed a similar general pattern as the bending and compressive strengths at 20 °C. All the FC's densities experienced a significant decrease in the split tensile strength after being subjected to 100 °C. The reduction ranged between 96% and 99%. Nevertheless, at 400 °C, the split tensile strength of all the densities decreased to between 66% and 72%. Furthermore, after being subjected to 800 °C, the FC's split tensile strength reduced considerably. The average residual split tensile strength decreased from 47% at 600 °C to 20% after exposure to
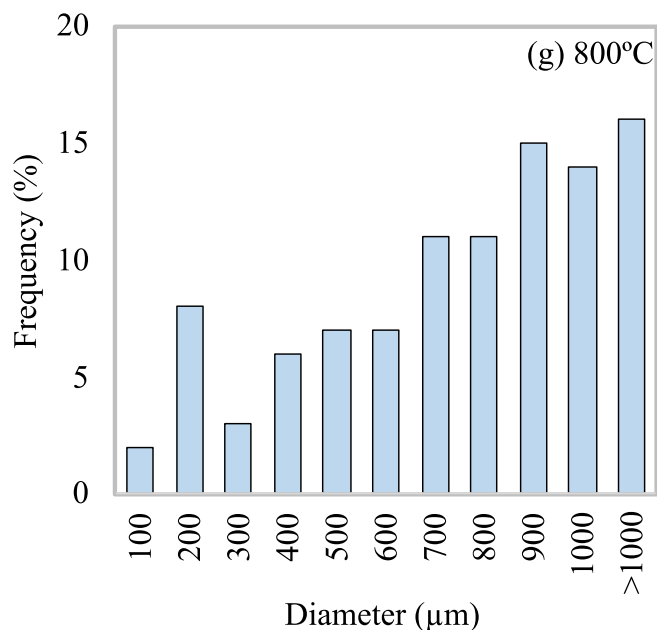
Fig. 30. (*continued*).

800 °C. This decrease was due to the decomposition of the hydration products. The same thermal treatment had a greater impact on the split tensile strength compared to the compressive strength. Since the impact of cracking coalescence on the split tensile strength was greater compared to the compressive strength, this was a primary reason for elevated temperatures, resulting in a greater reduction in the split tensile strength relative to the compressive strength. The growth, besides the initiation of each new crack, decreases the available load-carrying region, resulting in a rise in stresses at crack tips [63]. In addition, cracks start to seal up under compressive loads but open under tensile loads. The thermal incompatibility, hydration product decomposition, and high-water vapour pressure between aggregates and cement paste have a big effect on where cracks appear and how they grow from microcracks to macrocracks as the temperature rises.

4.9. Modulus of elasticity

Fig. 22 indicates the modulus of elasticity for various FC mixtures before and after exposure to elevated temperatures. The figure demonstrates that an increase in the density from 500 kg/m^3 to 1980 kg/m^3 led to a progressive decrease in the modulus of elasticity as temperature rose. As temperature increased, the influence of the density diminished gradually. At 100 °C–200 °C, the loss of the modulus of elasticity started owing to the deterioration of the microstructure and shrinkage of the paste caused by the evaporation of water. In addition, Fig. 23 displays the residual modulus of elasticity as a function of temperature. The residual modulus of elasticity rose as the density increased; thus, the effect became more pronounced as temperature rose. This behaviour was caused by a rise in the solid content as the density increased.

4.10. UPV

Fig. 24 demonstrates the UPV tests results for FC with varying densities (500 kg/m^3, 1000 kg/m^3, and 1500 kg/m^3) and mortar with a density of 1980 kg/m^3 at elevated and ambient temperatures. As exhibited in Fig. 24, the values of UPV of all the mixtures increased with temperatures up to 100 °C and then decreased, as reported in other investigations [64,65]. The outcomes ranged from 1991 m/s to 1429 m/s, 2417 m/s to 2007 m/s, 3115 m/s to 2632 m/s, and 3913 m/s to 3407 m/s for FC with densities of 500 kg/m^3, 1000 kg/m^3, and 1500 kg/m^3, and

mortar with a density of 1980 kg/m^3, respectively. The UPV enhancement ratios at 100 °C were 4.52%, 5.87%, 5.87%, and 4.01% for the mixtures with densities of 500 kg/m^3, 1000 kg/m^3, 1500 kg/m^3, and 1980 kg/m^3, respectively. The rise in the UPV values can be attributed to either the increased surface forces between particles of gel because of the gel's general stiffening or to the removed adsorbed water. Moreover, this noticed increase within UPV can be related to a progressive hydration procedure initiated by the prevalent temperature [66]. Castillo and Durrani [65] recorded similar behaviours. According to the authors' assessment, the observed increase within the phenomenon can be attributed to either the increase in interparticle surface forces or the overall cement gel reinforcement caused by the evaporation of absorbed moisture. It is noteworthy that the dehydration of FC will occur because of the evaporation process, which incorporates a fraction of the chemically bound water as well as the free water. At temperatures between 90 °C and 95 °C, the hydration procedure is initiated. In the range of 90 °C to 140 °C, a certain proportion of the chemically bound water will be discharged. Because of the calcium silicate hydrate (C-S-H) gel decomposition, certain amounts of water that is chemically bonded will also be lost. Nevertheless, the greatest decrease in UPV was observed within mixtures with a density of 500 kg/m^3, as was the case for the split tensile , bending, and compressive strengths. The mortar samples with a density of 1980 kg/m^3 possessed higher UPV outcomes compared to the other mixtures because of their decreasing porosity values and rising solid content. UPV is a representative for FC's defects such as cracks and pores. When the matrix contains honeycomb, pores, cracks, or any other defects, UPV decreases. Consequently, it can be used to determine the FC's quality.

4.11. Microstructural investigation

4.11.1. SEM analysis

To identify alterations in the FC and mortar's morphology, the SEM analysis was carried out on the mixtures with varying densities and high temperatures. Four mixtures were heated at 20 °C, 400 °C, and 600 °C, and five images were taken. The effects of various temperatures on the FC's microstructure with varying densities (500 kg/m^3, 1000 kg/m^3, and 1500 kg/m^3) and mortar with a density of 1980 kg/m^3 are depicted in Figs. 25, 26, 27, and 28, respectively. Fig. 25-b and 26-b demonstrate that FC with densities of 500 kg/m^3 and 1000 kg/m^3 exposed to 400 °C
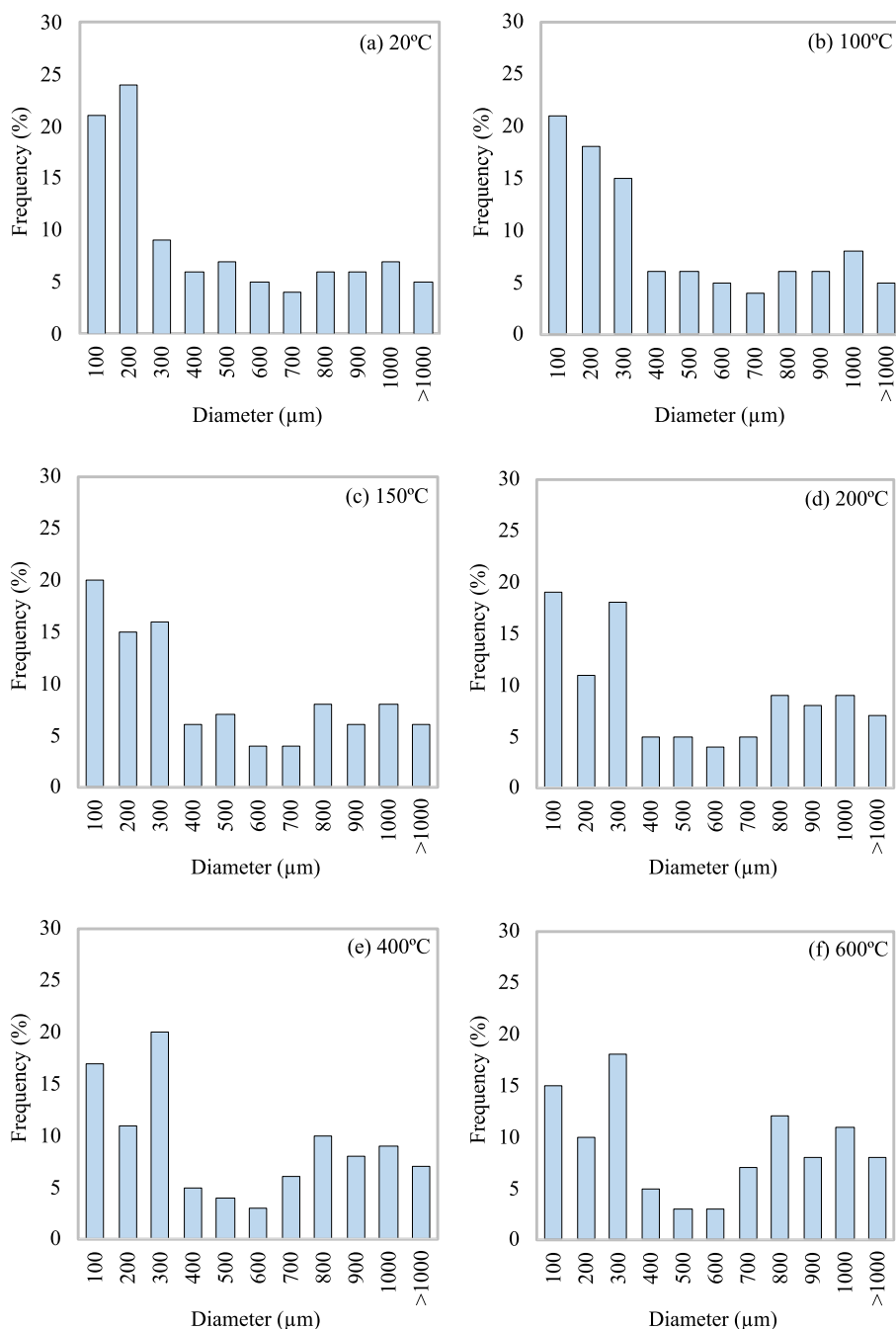
Fig. 31. Pore size distribution of FC specimens with a density of 1500 kg/m^3 exposed to various temperatures.

encountered a rise in the merged pores, pore diaphragm spalling, and crack dimensions in comparison to that at 20 °C. Nevertheless, the SEM results showed that FC with a density of 1500 kg/m^3 did not alter greatly within pores when exposed to 400 °C in comparison to the sample at ambient temperature, as displayed in Fig. 27(a-b). At these temperatures, portlandite broke down into water and lime [67 –69]. Because of the procedure of dehydration, a few pores and cracks also formed within the solid matrix. Fig. 26-c and 27-c illustrate a significant deterioration within the FC's microstructure exposed to 800 °C, particularly with a density of 500 kg/m^3. Alternatively, raising sold content while decreasing foam content raises the mortar's density. Consequently, it raises the solid matrix, enhances the pore distribution, and decreases the pore diameter (Fig. 25–a, 26–a, 27–a, and 28–a). The enhancement within the microstructure showed up in the increased FC's compressive strength as its density increased at ambient temperature.

4.12. Pore size distributions

For investigating the effect of the raised temperatures on the hydration reaction of cement-based materials, the pore distribution and porosity of FC-hardened pastes with different mortars and destinies can be used. In this regard, distinct pore distributions will affect the pastes' durability by influencing their impermeability and shrinkage [70]. The size, shape, and quantity of hydration products noticeably impact the pore and porosity distribution of hardened pastes. Figs. 29–32 exhibit the pore distribution of FC-hardened pastes with different densities and mortars following exposure to high temperatures. Reducing the foam content led to greater numbers of holes sized between 100–200 μm and
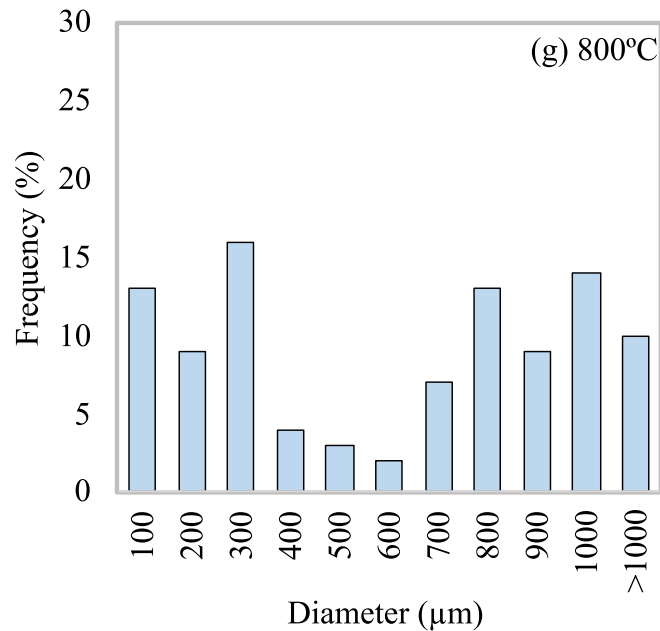
Fig. 31. (*continued*).

300–400 µm at 20 °C, but this trend reversed as the temperature rose. Within this range, the mortar specimen had the largest number of pores. The number of pores with widths greater than 400 µm was the lowest at both ambient temperature and increased temperature for the mortar specimen with a density of 1980 kg/m^3. The number of holes with sizes greater than 800 µm increased as temperature rose for all the specimens, with the greatest values seen in the specimens with a foam content of 500 kg/m^3. There were a few larger pores, and the number of them increased as the temperature and plastic density increased. This was because pores could overlap and merge at higher FC's densities (500 kg/m^3). Also, the FC's porosity increased evenly across all three densities because sulfoaluminate and C-S-H broke down at 300 °C and 200 °C. Besides, the observation of the calcium hydroxide disintegration into calcium oxide at temperatures greater than 400 °C could be explained by the increase in the porosity. The void size and distribution did not alter substantially when exposed to 600 °C in comparison to the samples at ambient temperature.

5. Conclusions

FC with varying densities (500 kg/m^3, 1000 kg/m^3, and 1500 kg/m^3) was compared to mortar with a density of (1980 kg/m^3) in terms of its behaviour at elevated temperatures. Experiments were conducted to determine the slump flow, mass loss, porosity, thermal conductivity, compressive strength, bending strength, split tensile strength, modulus of elasticity, UPV, and microstructure. Based on the evaluations' outcomes, the following conclusions can be drawn:

- As the FC's density increased, the slump values decreased. However, the impact of the mortar's density on reducing the slump was more significant than that of the FC's density. Besides, increasing the exposure temperature led to a deeper tone. Additionally, exposure to temperatures of 600 °C and 800 °C resulted in the exterior surface forming merged pores, spalling, and cracks.
- As the temperature increased, the specimens experienced a reduction in the mass loss. However, the densities of 1500 kg/m^3 for FC and 1980 kg/m^3 for mortar exhibited distinct variations. The rate of reduction lessened as the temperature rose from room temperature to 800 °C. This was also applicable to FC with a density of 1500 kg/m^3 and mortar with a density of 1980 kg/m^3 when the temperature

was under 400 °C. The mass loss decreased notably after reaching 400 °C, especially for mortar with a density of 1980 kg/m^3.

- The mortar and FC's porosity were mostly determined by density functions and were not greatly influenced by temperature. The change in the mechanical properties of mortar and FC at high temperatures was mainly caused by changes in the chemical composition of FC.
- As the temperature increased, the modulus of elasticity and compressive strength of the FC decreased consistently. Higher density improved the modulus of elasticity and residual compressive strength. After a longer exposure to 800 °C, the residual strength of mortar and FC decreased by 6.85% for 500 kg/m^3, 15.85% for 1000 kg/m^3, 25.48% for 1500 kg/m^3, and 18.75% for 1980 kg/m^3. The increased strength loss observed with a density of 500 kg/m^3 was due to a decrease in the solid matrix.
- Increasing temperature led to a gradual decrease in the split tensile and bending strengths of FC and mortar with different densities. At 800 °C, all the mixtures showed the lowest residual strengths; however, the mortar sample indicated the highest performance. While the UPV values for all the combinations increased when the temperature reached 100 °C and then declined.
- The decrease in the porosity led to an increase in the thermal conductivity for both mortar and FC as their density increased. However, the thermal conductivity for all the mixtures declined as temperature increased because of capillary fractures and the expansion and creation of voids within the material due to heat. Following exposure to 800 °C, the thermal conductivity of FC with different densities (500 kg/m^3, 1000 kg/m^3, and 1500 kg/m^3) fell by 86.18%, 42.42%, and 31.81%, respectively. However, the decrease for mortar with a density of 1980 kg/m^3 was 26.87%.
- As the temperature rose, the SEM data demonstrated a gradual increase in the level of degradation. At 400 °C, spalling and cracks appeared on the pore diaphragm with densities of 500 kg/m^3 and 1000 kg/m^3. The porous diaphragm displayed more temperature sensitivity than the solid matrix. Increasing the density of concrete improved its ability to withstand high temperatures by reducing the number of pores. As the temperature increased, the MIR analysis revealed a continuous rise in the percentage of pores, especially those over 1000 µm in size. Portlandite breakdown was initiated at 400 °C and concluded at 800 °C.
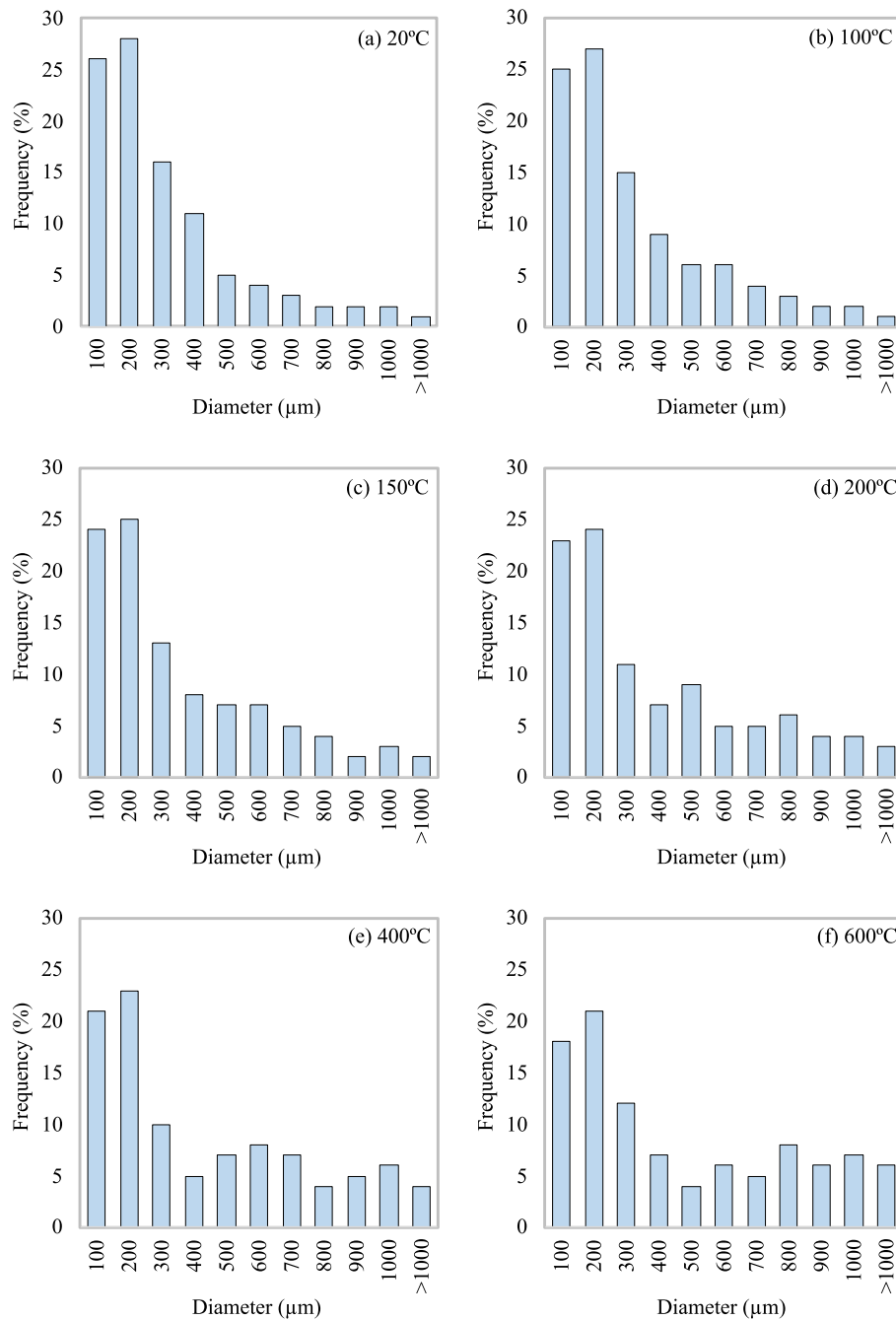
Fig. 32. Pore size distribution of mortar samples with a density of 1980 kg/m^3 exposed to various temperatures.

Despite the anticipated lower mechanical characteristics of FC compared to normal strength concrete, there is an opportunity for using low-density FC (500 kg/m^3) as fire-resistant partitions or load-bearing walls in low-rise residential construction. Rising the density of FC would enhance its specific heat capacity, enabling it to absorb more heat. This is positive for the application of FC in building construction as fire-resistant partitions.

CRediT authorship contribution statement

Md Azree Othuman Mydin: Writing – review & editing, Writing – original draft, Visualization, Validation, Supervision, Software, Resources, Project administration, Methodology, Investigation, Formal analysis, Data curation, Conceptualization. **Nadhim Hamah Sor:** Writing – review & editing, Writing – original draft, Visualization, Validation, Resources, Project administration, Formal analysis. **Alireza Bahrami:** Writing – review & editing, Writing – original draft, Visualization, Validation, Supervision, Software, Resources, Project administration, Methodology, Investigation, Formal analysis, Data curation, Conceptualization. **Anmar Dulaimi:** Writing – review & editing, Resources, Methodology, Investigation, Data curation. **Yasin Onuralp Özkılıç:** Writing – review & editing, Validation, Investigation. **Fadi Althoey:** Writing – review & editing, Validation, Formal analysis, Data curation. **P. Jagadesh:** Writing – review & editing, Software, Methodology, Formal analysis, Data curation. **Haytham F. Isleem:** Writing – review & editing, Writing – original draft, Visualization, Formal analysis, Data curation. **Taher A. Tawfik:** Writing – review & editing, Writing – original draft, Validation, Data curation.
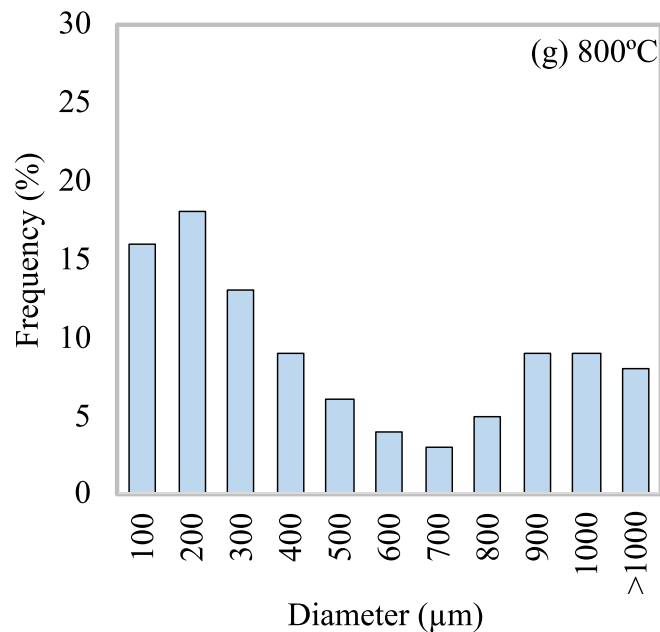
Fig. 32. (*continued*).

Declaration of Competing Interest

The authors declare that they have no known competing financial interests or personal relationships that could have appeared to influence the research work reported in this article.

Acknowledgement

References

[1] R.R. Agra, R. Serafini, A.D. de Figueiredo, Effect of high temperature on the mechanical properties of concrete reinforced with different fiber contents, Constr. Build. Mater. 301 (2021) 124242.

[2] T. Lee, G. Kim, G. Choe, E. Hwang, J. Lee, D. Ryu, J. Nam, Spalling Resistance of Fiber-Reinforced Ultra-High-Strength Concrete Subjected to the ISO-834 Standard Fire Curve: Effects of Thermal Strain and Water Vapor Pressure, Materials 13 (2020) 3792.

[3] EN 1992-1-2; Eurocode 2: Design of Concrete Structures-Part 1–2: General Rules-Structural Fire Design. The European Union: Mestreech, The Netherlands, **1992**.

[4] M.H. Nensok, H. Awang, Investigation of thermal, mechanical and transport properties of ultralightweight foamed concrete (ULFC) strengthened with alkali treated banana fibre, J. Adv. Res. Fluid Mech. Therm. Sci. 86 (1) (2021) 123–139.

[5] J.M. Abed, B.A. Khaleel, I.S. Aldabagh, N.H. Sor, The effect of recycled plastic waste polyethylene terephthalate (PET) on characteristics of cement mortar, J Phys Conf 1973 (1) (2021, August;) 012121.

[6] A.F. Phius, N.M. Sani, N.M. Tawil, Potential of Green Construction in Malaysia: Industrialised Building System (IBS) vs Traditional Construction Method, E3S Web Conf. 3 (2014) 01009.

[7] M.F. Mohamed Shajahan, S. Ganesan, N.M. Sani, Laboratory investigation on compressive strength and micro-structural features of foamed concrete with addition of wood ash and silica fume as a cement replacement, MATEC Web Conf. 17 (2014) 01004.

[8] M.A.O. Mydin, N.H. Sor, F. Althoey, Y.O. Özkılıç, M.M.A.B. Abdullah, H.F. Isleem, T.A. Tawfik, Performance of lightweight foamed concrete partially replacing cement with industrial and agricultural wastes: Microstructure characteristics, thermal conductivity, and hardened properties, Ain Shams Eng. J. 14 (11) (2023) 102546.

[9] A.A. Mohammed, T.A. Tawfik, A.S. Aadi, N. Hamah Sor, Ultra-high performance of eco-friendly self-compacting concrete incorporated cement Kiln dust with/without waste plastic and polypropylene fiber, Innovative Infrastructure Solutions 8 (3) (2023) 94.

[10] A. Driouich, S.A. El Hassani, N.H. Sor, Z. Zmirli, M.A.O. Mydin, A. Aziz, H. Chaair, Mix design optimization of metakaolin-slag-based geopolymer concrete synthesis using RSM, Results in Engineering 20 (2023) 101573.

[11] M.I. Al Biajawi, M.F. Abdulrahman, W.M. Saod, N. Hilal, R. Embong, N.H. Sor, Investigation the effect of nanocarbon tube prepared from tea waste on microstructure and properties of cement mortar, Environ. Sci. Pollut. Res. (2023) 1–14.

[12] M.A.O. Mydin, M.M.A.B. Abdullah, N.H. Sor, R. Omar, A. Dulaimi, P.O. Awoyera, A.F. Deifalla, Thermal conductivity, microstructure and hardened characteristics of foamed concrete composite reinforced with raffia fiber, J. Mater. Res. Technol. (2023).

[13] E. Serri, M.Z. Suleiman, M.A.O. Mydin, The effects of oil palm shell aggregate shape on the thermal properties and density of concrete, Adv. Mat. Res. 935 (2014) 172–175.

[14] N. Mohamad, A.A.A. Samad, M.T. Lakhiar, M.A. Othuman Mydin, S. Jusoh, A. Sofia, S.A. Efendi, Effects of Incorporating Banana Skin Powder (BSP) and Palm Oil Fuel Ash (POFA) on Mechanical Properties of Lightweight Foamed Concrete, Int. J. Int. Eng. 10 (2018) 69–76.

[15] S. Ganesan, M.A. Othuman Mydin, N.M. Sani, A.I. Che Ani, Performance of polymer modified mortar with different dosage of polymeric modifier, MATEC Web Conf. 15 (2014) 01039.

[16] E.K.K. Nambiar, K. Ramamurthy, Air-void characterisation of foam concrete, Cem. Concr. Res. 37 (2007) 221–230.

[17] O. Zaid, N.A.H. Sor, R. Martínez-García, J. de Prado-Gil, K.M. Elhadi, A.M. Yosri, Sustainability evaluation, engineering properties and challenges relevant to geopolymer concrete modified with different nanomaterials: A systematic review, Ain Shams Eng. J. 102373 (2023).

[18] M.A. Tambichik, A.A. Abdul Samad, N. Mohamad, A.Z. Mohd Ali, M.A. Othuman Mydin, M.Z. Mohd Bosro, M.A. Iman, Effect of combining Palm Oil Fuel Ash (POFA) and Rice Husk Ash (RHA) as partial cement replacement to the compressive strength of concrete, Int. J. Integr. Eng. 10 (2018) 61–67.

[19] K. Dhasindrakrishna, S. Ramakrishnan, K. Pasupathy, J. Sanjayan, Collapse of fresh foam concrete: Mechanisms and influencing parameters, Cem. Concr. Compos. 122 (2021) 104151.

[20] N.M. Zamzani, A.N.A. Ghani, Experimental data on compressive and flexural strengths of coir fibre reinforced foamed concrete at elevated temperatures, Data Brief 25 (2019) 104320.

[21] H. Awang, M.A.O. Mydin, A.F. Roslan, Effects of fibre on drying shrinkage, compressive and flexural strength of lightweight foamed concrete, Adv. Mat. Res. 587 (2012) 144–149.

[22] W.M. Lin, T.D. Lina, L.J. Powers-Couche, Microstructures of fire-damaged concrete, J. Am. Concr. Inst. Mater. 93 (1996) 199–205.

[23] Y. Li, E.-H. Yang, K.H. Tan, Flexural behavior of ultra-high performance hybrid fiber reinforced concrete at the ambient and elevated temperature, Constr. Build. Mater. 250 (2020) 118487.

[24] F. Althoey, N.H. Sor, H.M. Hadidi, S.F.A. Shah, A. Alaskar, S.M. Eldin, M.F. Javed, Crack Width Prediction of Self-Healing Engineered Cementitious Composite Using multi-expression programming, J. Mater. Res. Technol. (2023).

[25] R. Serafini, S.R. Dantas, R.P. Salvador, R.R. Agra, D.A. Rambo, A.F. Berto, A.D. de Figueiredo, Influence of fire on temperature gradient and physical-mechanical properties of macro-synthetic fiber reinforced concrete for tunnel linings, Constr. Build. Mater. 214 (2019) 254–268.

[26] N. Hua, N.E. Khorasani, A. Tessari, R. Ranade, Experimental study of fire damage to reinforced concrete tunnel slabs, Fire Saf. J. 127 (2022) 103504.

[27] R. Serafini, A. de La Fuente, A.D. de Figueiredo, Assessment of the post-fire residual bearing capacity of FRC and hybrid RC-FRC tunnel sections considering thermal spalling, Mater. Struct. 54 (2021) 219.

[28] Kearsley, E.P.; Mostert, H.F. The use of foamed concrete in refractories. In Use of Foamed Concrete in Construction; Thomas Telford: London, UK, 2005; pp. 89–96.

[29] M.A. Othuman, Y.C. Wang, Elevated-temperature thermal properties of lightweight foamed concrete, Constr. Build. Mater. 25 (2011) 705–716.

[30] A.F. Bingöl, R. Gül, Effect of elevated temperatures and cooling regimes on normal strength concrete, Fire Mater. 33 (2008) 79–88.

[31] W. Botte, R. Caspeele, Post-cooling properties of concrete exposed to fire, Fire Saf. J. 92 (2017) 142–150.

[32] G.G. Carette, K.E. Painter, V.M. Malhotra, Sustained high temperature effects on concrete made with normal Portland cement, normal Portland cement and slag, or normal Portland cement and fly ash, Concr. Int. 4 (1982) 41–51.

[33] X. Tan, W. Chen, J. Wang, D. Yang, X. Qi, Y. Ma, X. Wang, S. Ma, C. Li, Influence of high temperature on the residual physical and mechanical properties of foamed concrete, Constr. Build. Mater. 135 (2017) 203–211.

[34] O.Y. Bayraktar, G. Kaplan, O. Gencel, A. Benli, M. Sutcu, Physico-mechanical, durability and thermal properties of basalt fiber reinforced foamed concrete containing waste marble powder and slag, Constr. Build. Mater. 288 (2021) 123128.

[35] M.A.O. Mydin, Y.C. Wang, An experimental investigation of mechanical properties of lightweight foamed concrete subjected to elevated temperatures up to 600° C, CRL Letters 1, no. 4 (2010).

[36] BS EN 197-1. Cement - Composition, specifications and conformity criteria for common cements. British Standards Institute: London, UK; 2011.

[37] ASTM C33-03. Standard Specification for Concrete Aggregates. American Society for Testing and Materials. West Conshohocken, PA: ASTM International; 2003.

[38] BS EN 3148. Water for Making Concrete (Including Notes on the Suitability of the Water). British Standards Institute: London, UK; 1980.

[39] ISO 834-1. Fire Resistance Test - Elements of Building Construction - Part 1: General Requirements, International Standards ISO 834, Geneva, Switzerland; 1999.

[40] V.K.R. Kodur, S. Banerji, R. Solhmirzaei, Test methods for characterizing concrete properties at elevated temperature, Fire Mater. 44 (3) (2020) 381–395.

[41] BS EN 12390-3. Testing Hardened Concrete. Compressive Strength of Test Specimens. British Standards Institute: London, UK; 2011.

[42] BS EN 12390-5. Testing Hardened Concrete. Flexural Strength of Test Specimens. British Standards Institute: London, UK; 2019.

[43] BS EN 12390-6. Testing Hardened Concrete. Tensile Splitting Strength of Test Specimens. British Standards Institute: London, UK, 2009.

[44] ASTM C469. Standard Test Method for Static Modulus of Elasticity and Poisson's Ratio of Concrete in Compression. American Society for Testing and Materials: West Conshohocken, PA: ASTM International; 2002.

[45] ASTM C177-19. Standard Test Method for Steady-State Heat Flux Measurements and Thermal Transmission Properties by Means of the Guarded-Hot-Plate Apparatus. American Society for Testing and Materials: West Conshohocken, PA: ASTM International; 2019.

[46] BS EN 12504-4. Testing concrete. Determination of ultrasonic pulse velocity. British Standards Institute: London, UK; 2021.

[47] P. Onprom, K. Chaimoon, R. Cheerarot, Influence of bottom ash replacements as fine aggregate on the property of cellular concrete with various foam contents, Adv. Mater. Sci. Eng. 2015 (2015).

[48] Z. Huang, et al., Evaluation of compressive behavior of ultra-lightweight cement composite after elevated temperature exposure, Constr. Build. Mater. 148 (2017) 579–589.

[49] Y. Ding, et al., Influence of different fibers on the change of pore pressure of self-consolidating concrete exposed to fire, Constr. Build. Mater. 113 (2016) 456–469.

[50] H. Mohammadhosseini, et al., Performance evaluation of novel prepacked aggregate concrete reinforced with waste polypropylene fibers at elevated temperatures, Constr. Build. Mater. 259 (2020).

[51] A.A. Awal, I. Shehu, Performance evaluation of concrete containing high volume palm oil fuel ash exposed to elevated temperature, Constr. Build. Mater. 76 (2015) 214–220.

[52] Y. Wang, et al., Effect of elevated temperatures and cooling methods on strength of concrete made with coarse and fine recycled concrete aggregates, Constr. Build. Mater. 210 (2019) 540–547.

[53] M.A. Othuman Mydin, Y.C. Wang, Thermal and mechanical properties of lightweight foamed concrete at elevated temperatures, Mag. Concr. Res. 64 (3) (2012) 213–224.

[54] M. Mydin, Y. Wang, Mechanical properties of foamed concrete exposed to high temperatures, Constr. Build. Mater. 26 (1) (2012) 638–654.

[55] M.R. Ahmad, B. Chen, Experimental research on the performance of lightweight concrete containing foam and expanded clay aggregate, Compos. B Eng. 171 (2019) 46–60.

[56] A.A. Sayadi, J.V. Tapia, T.R. Neitzert, G.C. Clifton, Effects of expanded polystyrene (EPS) particles on fire resistance, thermal conductivity and compressive strength of foamed concrete, Constr. Build. Mater. 112 (2016) 716–724.

[57] F. Koksal, Y. Sahin, O. Gencel, Influence of expanded vermiculite powder and silica fume on properties of foam concretes, Constr. Build. Mater. 257 (2020) 119547.

[58] H. Weigler, S. Karl, Structural lightweight aggregate concrete with reduced density- lightweight aggregate foamed concrete, Int. J. Cem. Compos. Light. Concr. 2 (1980) 101–104, https://doi.org/10.1016/0262-5075(80)90029-9.

[59] T.A. Holm, J.P. Ries, Lightweight concrete and aggregates, vol. 169, ASTM Special Techn. Publ. (1994) 522–532.

[60] Chandra, S., Berntsson, L., Lightweight Aggregate Concrete, Noyes Publications/William Andrew, Norwich, NY, 2002. ISBN no. 081551486-7.

[61] A.H. Akca, N. Ozyurt, Effects of re-curing on microstructure of concrete after high temperature exposure, Constr. Build. Mater. 168 (2018) 431–441.

[62] N. Farzadnia, et al., Characterization of high strength mortars with nano Titania at elevated temperatures, Constr. Build. Mater. 43 (2013) 469–479.

[63] E.T. Dawood, et al., Behavior of foamed concrete reinforced with hybrid fibers and exposed to elevated temperatures, SN Appl. Sci. 2 (1) (2020) 84.

[64] A.M. Neville, Properties of Concrete, John Wiley & Sons, New York, 1997.

[65] C. Castillo, A.J. Durrani, Effect of transient high temperature on high strength concrete, ACI Mater. J. 87 (1) (1990) 47–53.

[66] W.F. Chen, Plasticity in Reinforced Concrete, McGraw-Hill, New York, 1982, p. 474.

[67] U. Schneider, et al., Effect of temperature on steel and concrete for PCRV's, Nucl. Eng. Des. 67 (2) (1982) 245–258.

[68] M. Heikal, et al., Behavior of composite cement pastes containing microsilica and fly ash at elevated temperature, Constr. Build. Mater. 38 (2013) 1180–1190.

[69] P. Jagadesh, S. Oyebisi, A.H. Muthu, A. Sarulatha, K. Supikshaa, N.A. Sor, M.A.O. Mydin, Recycled concrete powder on cement mortar: Physico-mechanical effects and lifecycle assessments, J. Build. Eng. 86 (2024) 108507.

[70] B. Das, B. Kondraivendhan, Implication of pore size distribution parameters on compressive strength, permeability and hydraulic diffusivity of concrete, Constr. Build. Mater. 28 (2012) 382–386.